Article

Not peer-reviewed version

Multi-Omics Profiling Exposes a Metabolic Void in Prostate Cancer Models That Drives Precursor Dependence and Clinical Progression

Jibira Yakubu , Therina du Toit , Amit V. Pandey *

Posted Date: 10 April 2026

doi: 10.20944/preprints202604.0750.v1

Keywords: castration-resistant prostate cancer; intracrine steroidogenesis; androgen receptor signaling; lineage plasticity; metabolic rewiring; liquid chromatography-mass spectrometry; multi-omics; precursor conversion

 doi:10.20944/preprints202604.0750.v1

Article

Multi-Omics Profiling Exposes a Metabolic Void in Prostate Cancer Models That Drives Precursor Dependence and Clinical Progression

Jibira Yakubu [1,2,3], Therina du Toit [2,4] and Amit V. Pandey [1,2,*]

[1] Pediatric Endocrinology, Diabetology and Metabolism, University Children's Hospital, Inselspital, Bern, Switzerland.

[2] Translational Hormone Research Program, Department of Biomedical Research, Faculty of Medicine, University of Bern, Bern, Switzerland.

[3] Graduate School for Cellular and Biomedical Sciences, University of Bern, Bern, Switzerland.

[4] Department of Nephrology and Hypertension, University Hospital Bern, Inselspital, University of Bern, Bern, Swtizerland

* Correspondence: amit.pandey@unibe.ch; Tel.: 0041 31 632 9637

Abstract

Castration-resistant prostate cancer (CRPC) survives androgen deprivation, a mechanism widely attributed to autonomous *de novo* steroidogenesis. Despite the clinical deployment of CYP17A1 inhibitors, the metabolic fidelity of the models underpinning this "tumor-as-gonad" dogma remains controversial. Here, integrating high-resolution liquid chromatography-mass spectrometry with transcriptomics across diverse prostate cancer models, we demonstrate that malignant cell lines universally lack autonomous steroidogenic capacity due to the transcriptional silencing of *CYP17A1*. Instead, these models operate as high-efficiency precursor "converters" by upregulating *HSD3B1* and *AKR1C3*. Clinical stratification of 844 Prostate Adenocarcinoma patients corroborated this precursor-dependent phenotype. We identify a critical divergence: AR-High tumors rely on oxidative phosphorylation, whereas the transition to an AR-Low state is marked by extensive lineage plasticity. Strikingly, a neuroendocrine plasticity score inversely correlates with AR flux and independently predicts clinical progression (HR=2.41, p=0.024). Our findings redefine CRPC metabolism, dictating a therapeutic shift toward targeting downstream precursor conversion and adaptive lineage plasticity.

Keywords: castration-resistant prostate cancer; intracrine steroidogenesis; androgen receptor signaling; lineage plasticity; metabolic rewiring; liquid chromatography-mass spectrometry; multi-omics; precursor conversion

Introduction

Prostate cancer (PCa) growth and survival are critically dependent on androgen receptor (AR) signaling. Since the pioneering work of Charles Huggins and Clarence Hodges in 1941, which established the androgen-dependence of prostatic epithelium, Androgen Deprivation Therapy (ADT) has served as the cornerstone of systemic management for advanced disease. Although initially effective, most patients inevitably progress to castration-resistant prostate cancer (CRPC), a lethal stage characterized by persistent AR activity despite low circulating androgen levels [1–3]. This highlights the remarkable adaptability of AR signaling and the importance of understanding its regulation in both normal and malignant prostate cancer. One major therapeutic advance in CRPC has been the development of abiraterone acetate, a potent inhibitor of CYP17A1, a key enzyme in androgen biosynthesis. By suppressing adrenal and intratumoral androgen production, abiraterone significantly prolongs survival in metastatic CRPC patients [4–6]. However, resistance to abiraterone

 doi:10.20944/preprints202604.0750.v1

invariably emerges, underscoring the remarkable adaptability of androgen signaling in prostate cancer. Multiple mechanisms of abiraterone resistance have been proposed, including AR amplification or mutation, the expression of constitutively active AR splice variants (AR-V7 & Splice variants), upregulation of steroidogenic enzymes, and the activation of bypass signaling pathways [1,2,7,8]. Increasing evidence suggests that CRPC tumors can sustain androgen signaling through intratumoral steroidogenesis, converting cholesterol or adrenal precursors into potent androgens such as testosterone and dihydrotestosterone (DHT), even under pharmacologic CYP17A1 inhibition [9].

The concept that a prostate tumor can function as a pseudo-gonad or pseudo-adrenal organ has driven the development of CYP17A1 inhibitors; however, the precise biochemical fidelity of this pathway in standard research models remains contentious. Previous studies utilizing radiolabeled substrates in xenograft models suggested a robust capacity for *de novo* synthesis from cholesterol. In contrast, subsequent investigations utilizing high-sensitivity mass spectrometry in cell culture models have failed to detect significant flux through the early steps of steroidogenesis, suggesting that these models may be metabolically broken or reliant on specific precursors. Furthermore, the contribution of the glucocorticoid axis, specifically the loss or gain of cortisol synthesis and metabolism, has emerged as a potential determinant of tumor differentiation and drug resistance, yet a systematic characterization of this pathway across diverse PCa models is lacking.

Preclinical prostate cancer cell models have played a crucial role in elucidating the mechanisms of resistance to treatment. Androgen-sensitive lines such as LNCaP, as well as more androgen-independent models including 22Rv1, VCaP, and DU145, display marked heterogeneity in AR status, steroidogenic capacity, and response to hormonal manipulation. 22Rv1 and VCaP cells are known to express AR splice variants and retain androgen responsiveness under castrate conditions, while DU145 cells lack functional AR signaling [10–17]. Normal prostate epithelial cells (RWPE-1) [18] serve as non-malignant comparators, whereas adrenal-derived H295R cells are a well-established model of comprehensive steroid biosynthesis [19–24]. While these models provide essential mechanistic insights, their clinical fidelity in distinguishing between autonomous steroidogenesis and precursor conversion remains a subject of intense debate. Specifically, the transcriptomic and metabolic architecture of these models must be linked with the large-scale multi-omics landscapes observed in clinical cohorts to identify the biological drivers of lethal progression.

Despite extensive study, a systematic, multi-layered comparison of steroid production, transcriptomic alterations, and functional androgen dependence across diverse prostate cancer models remains limited. In particular, the mechanisms underlying differential androgen responsiveness among androgen-sensitive and androgen-insensitive cell lines have not been fully elucidated. Also, the prognostic significance of these transcriptomic archetypes characterized by a shift from androgen-driven bioenergetics to lineage plasticity is poorly defined in the clinical setting.

In this study, we characterized a panel of androgen-sensitive and androgen-insensitive prostate cancer cell lines, along with normal prostate epithelial cells and an adrenal steroidogenic cell line, using RNA sequencing, LC-MS-based steroid profiling, and cell viability assays in the presence or absence of dihydrotestosterone (DHT). To validate the clinical relevance of our cell line data, we integrated these multi-omics signatures with a comprehensive dataset of 844 PRAD samples from the Genomic Data Commons (GDC). By quantifying AR regulatory flux via transcription factor inference and mapping lineage plasticity through Gene Set Variation Analysis (GSVA), we evaluated the independent prognostic value of these molecular states in predicting progression-free interval (PFI). Our analysis provides a comprehensive assessment of steroidogenic capacity and AR signaling plasticity across prostate cancer phenotypes, offering mechanistic and clinical insights into the regulation of androgen-dependent growth and the emergent metabolic dependencies that drive therapeutic resistance.

 doi:10.20944/preprints202604.0750.v1

Materials and Methods

Cell Lines and Culture Conditions

Human prostate cancer cell lines LNCaP (FGC; ATCC® CRL-1740), VCaP (ATCC® CRL-2876), PC3 (ATCC® CRL-1435), DU145 (ATCC® HTB-81), and the non-malignant prostate epithelial cell line RWPE-1 (ATCC® CRL-11609 / CRL-3607) were obtained from the American Type Culture Collection (ATCC®; Manassas, VA, USA). Cell lines were authenticated and routinely tested for mycoplasma contamination. Passage numbers during all experiments were maintained below 30. LNCaP and PC3 cells were maintained in RPMI-1640 medium supplemented with 2 mM L-glutamine, 10 mM HEPES, 1 mM sodium pyruvate, 10% fetal bovine serum (FBS), and 1% penicillin–streptomycin (Gibco™, Thermo Fisher Scientific, Waltham, MA, USA). VCaP and DU145 cells were cultured in Dulbecco's Modified Eagle Medium (DMEM) supplemented with 10% FBS, 1% antibiotic mix (100×), and 1 mM sodium pyruvate. RWPE-1 cells were maintained in keratinocyte serum-free medium supplemented with 0.05 mg/mL bovine pituitary extract, 5 ng/mL human recombinant epidermal growth factor, and 1% penicillin–streptomycin (Gibco™, Thermo Fisher Scientific). Human adrenocortical carcinoma NCI-H295R (ATCC® CRL-2128) cells were cultured in DMEM/Ham's F-12 medium containing L-glutamine and 15 mM HEPES (Thermo Fisher Scientific), supplemented with 5% NU-I serum (Becton Dickinson, Franklin Lakes, NJ, USA), 0.1% insulin–transferrin–selenium (ITS; 100 U/mL), and 1% penicillin–streptomycin [25,26].

DHT Treatment and Cell Viability Assays

To assess androgen dependence, PCa cells (LNCaP, DU145, PC3, VCaP, and 22RV1) and RWPE-1 cells were seeded at a density of 1×10^4 cells/well in complete culture medium, CSS-medium, and CSS-medium supplemented with 0.01% $^{v}/_{v}$ ethanol or 10 nM dihydrotestosterone (DHT). Cell proliferation was assessed after 24, 48, and 72 hours using a Resazurin metabolic assay [25,27,28]. The relative fluorescent values were normalized to those of vehicle-treated controls. Experiments were performed with at least three biological replicates, each measured in technical triplicate.

Steroid Extraction and LC–MS Analysis

For steroid analysis, NCI H295R cells and PCa cells were treated with 1 µM pregnenolone for 24 h. Steroids were measured by a Liquid Chromatography–High-Resolution Mass Spectrometry (LC-HRMS) method, as previously described and validated [27]. Briefly, steroids were extracted from 500 µL cell media aliquots and 38 µL of a mixture of internal standards (at 3.8 nM each) using solid-phase extraction with an OasisPrime HLB 96-well plate. Samples were resuspended in 100 µL 33% methanol, and 20 µL was injected into the LC-HRMS instrument (Vanquish UHPLC coupled to a Q Exactive Orbitrap Plus, from Thermo Fisher Scientific, Waltham, MA, USA) using an Acquity UPLC HSS T3 column (from Waters, Milford, MA, USA). Data from the mass spectrometer were processed using TraceFinder 4.0 (from Thermo Fisher, Waltham, MA, USA).

RNA Extraction and RNA Sequencing

Total RNA was extracted using the Direct-zol RNA kit (Zymo Research Corp., Irvine, CA, USA) according to the manufacturer's protocol. RNA integrity and concentration were assessed by Novogene (Cambridge, UK) using capillary electrophoresis and fluorometric quantification prior to library preparation. Only samples with RIN ≥ 7.0 were retained for sequencing. Approximately 40 million strand-specific paired-end reads (150 bp) were generated per sample. Poly(A)-enriched mRNA libraries were constructed and sequenced on an Illumina NovaSeq X Plus platform, generating 150 bp paired-end reads.

 doi:10.20944/preprints202604.0750.v1

Differential Gene Expression and Pathway Analysis

Gene expression quantification was performed using FeatureCounts or equivalent transcript-level quantification tools. Although differential expressions would typically be assessed using statistical frameworks such as DESeq2, the absence of biological replicates in this experiment prevented robust statistical inference. Accordingly, genes were not classified as significantly up- or downregulated based on adjusted p-values. Instead, analysis proceeded descriptively at the pathway level. To contextualize functional variation between prostate cancer cell lines, pathway enrichment analyses were performed using Gene Set Enrichment Analysis (GSEA) in conjunction with KEGG, Reactome, Disease Ontology, DisGeNET, and Gene Ontology (GO) databases. Emphasis was placed on pathways associated with steroid biosynthesis, cholesterol metabolism, androgen receptor (AR) signaling, and prostate cancer–related disease pathways. Gene expression values were log2-transformed and variance-filtered prior to visualization. Exploratory unsupervised clustering was performed using heatmaps and principal component analysis (PCA) generated via the pheatmap and ggplot2 packages in R.

A Systematic Multi-Omic Analysis of the GDC PRAD Dataset

To characterize the multi-omic profile of the Prostate Adenocarcinoma (PRAD) cohort, a comprehensive dataset of 844 samples was retrieved from the Genomic Data Commons (GDC) Data Portal, integrating transcriptomic data with clinical metadata [29,30]. Following standardized pre-processing and normalization using the limma (v3.62.0) package [31]. To categorize AR activity, samples were stratified into AR-high and AR-low groups based on the median GSVA score of a validated Androgen Receptor signaling signature [32]. To move beyond transcript abundance, transcription factor (TF) activity inference was performed using the decoupleR package to quantify AR regulatory flux. The integration of specific metabolic dependences was visualized using a multiomic heatmap generated via ComplexHeatmap (v2.22.0). The heatmap displays z-score-normalized expression values for key metabolic and signaling regulators, clustered alongside clinical annotations and GSVA scores for AR, Ferroptosis, and steroid activity. Furthermore, a lineage Plasticity Score was generated via GSVA (v1.54.0) to identify shifts toward neuroendocrine-like states. Statistical significance for differential expressions was determined using an FDR-adjusted p-value <0.05 and a [$\log_2$ FC ≥ 1.0]. Functional drivers were identified using GSEA and ORA via clusterProfiler (v4.14.0), targeting MSigDB Hallmark and KEGG databases [33]. The prognostic significance of these signatures was evaluated using Progression-Free Interval (PFI) data via univariable and multivariable Cox proportional hazards models and Kaplan-Meier curves using the survival (v3.7-0) and survminer (v0.5.0) packages. All computations were performed in the R environment (v4.4.2).

Statistical Analysis

All quantitative measurements are presented as mean ± SEM unless otherwise indicated. Statistical analysis for viability assays was performed using GraphPad Prism *version 10* or R. Comparisons involving two groups were conducted using Student's t-tests, whereas multi-group comparisons utilized one-way or two-way ANOVA with appropriate post hoc tests (Tukey's multiple comparison). A p-value < 0.05 was considered statistically significant, and data reflect three independent experimental replicates. One-way ANOVA with Tukey's post hoc test demonstrated significant reductions in viability under charcoal-stripped serum (CSS) conditions relative to complete medium, indicating androgen dependence. Dihydrotestosterone (DHT) supplementation restored growth in AR-positive prostate cancer lines ($p < 0.001$), confirming the functional responsiveness of AR signaling in these models. Collectively, these data validate the experimental framework for probing androgen-regulated pathways and highlight the central contribution of AR signaling to prostate cancer cell proliferation.

 doi:10.20944/preprints202604.0750.v1

Results

1. Differential Androgen Dependence Revealed by DHT Supplementation Assays

To establish an experimental baseline for androgen responsiveness, we first characterized a panel of prostate-derived cell lines representing androgen-sensitive, androgen-insensitive, and non-malignant phenotypes. Parental LNCaP, 22Rv1, and VCaP cells demonstrated clear AR-dependent growth behavior, consistent with their reliance on AR signaling for proliferation. In contrast, DU145 cells, which lack functional AR, displayed minimal sensitivity to androgen manipulation, while RWPE-1 served as a non-malignant prostate epithelial reference. Cell viability was measured under complete medium, androgen-depleted medium (CSS), or CSS supplemented with 10 nM dihydrotestosterone (DHT) over 24–72 hours. One-way ANOVA performed independently for each cell line and time point revealed a significant treatment effect in all AR-positive lines at 48 and 72 hours ($p < 0.001$) (*Table S1*). By comparison, DU145 cells showed no significant difference between treatments at 24 hours ($p = 0.106$), reinforcing their androgen-independent phenotype. Androgen deprivation markedly reduced viability in the AR-positive models, whereas DHT supplementation restored proliferative capacity to levels comparable to those in complete medium, indicating sustained androgen responsiveness. RWPE-1 cells also exhibited condition-dependent changes in viability, though with distinct kinetics compared with malignant cell lines. Together, these data demonstrate that androgen availability exerts a dominant and time-dependent influence on prostate cell proliferation, with effects tightly coupled to AR signaling status.

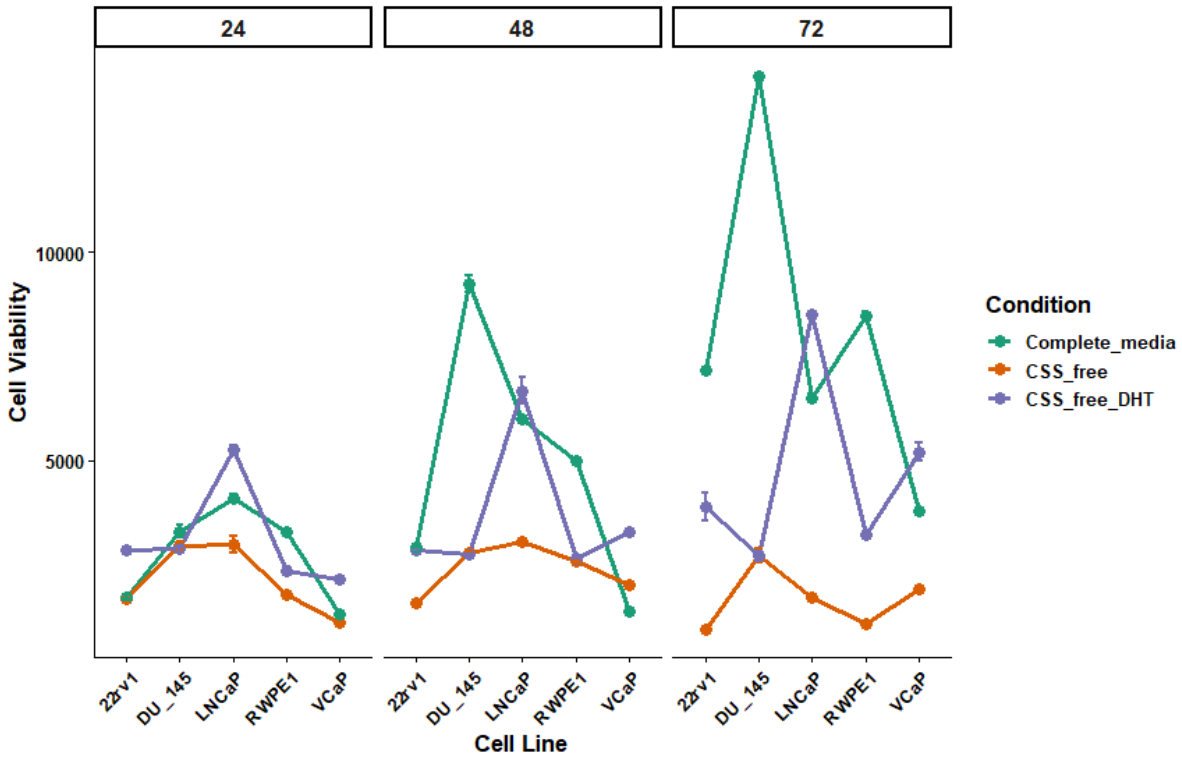

Figure 1. Androgen-dependent viability of prostate cell lines under distinct culture conditions. Cell viability was measured in parental prostate cancer cell lines (LNCaP, 22Rv1, VCaP, DU145) and non-malignant RWPE-1 cells cultured for 24, 48, and 72 hours in complete medium, charcoal-stripped serum (CSS)-free medium, or CSS-free medium supplemented with 10 nM dihydrotestosterone (DHT). Data represent mean ± SEM from triplicate experiments. One-way ANOVA, performed separately for each cell line and time point, revealed significant treatment effects ($p < 0.001$ for AR-positive lines at 48 and 72 h). Post-hoc Tukey's tests showed that DHT supplementation significantly rescued viability compared to CSS-free medium (adjusted $p < 0.05$ to $p < 0.001$) (Table S1). DU145 cells showed no significant change in viability at 24 hours, consistent with AR negativity. NB: DU145 (DU_145).

 doi:10.20944/preprints202604.0750.v1

2. LC–MS Profiling Reveals Heterogeneous Steroidogenic Capacity in Prostate Cancer Cells

To directly quantify steroid biosynthesis across models, we performed LC-MS-based steroid profiling under androgen-depleted culture conditions. As expected, H295R adrenocortical carcinoma cells produced a broad panel of steroid precursors and active androgens, validating assay sensitivity and dynamic range (*Figure 2A*). Heatmap visualization of log-transformed steroid abundances revealed pronounced differences across all models (*Figure 2B*). H295R cells formed a separate cluster, driven by high production of multiple steroid species, whereas prostate-derived cells displayed heterogeneous steroid output. RWPE-1 cells produced minimal steroid intermediates, consistent with limited steroidogenic capacity in non-malignant prostate epithelium. In contrast, prostate cancer cell lines LNCaP and VCaP generated detectable androgen precursors (DHEA) and downstream androgens, suggesting partial steroidogenic competence. Principal component analysis (PCA) further resolved these differences, with H295R cells separating along the first principal component due to elevated steroid production, while prostate cancer models occupied more intermediate positions. The LC–MS heatmap and PCA analyses provide a global assessment of steroid biosynthesis, supporting a role for cell-intrinsic androgen metabolism and precursor utilization in prostate cancer, with implications for intratumoral androgen maintenance during therapeutic pressure.

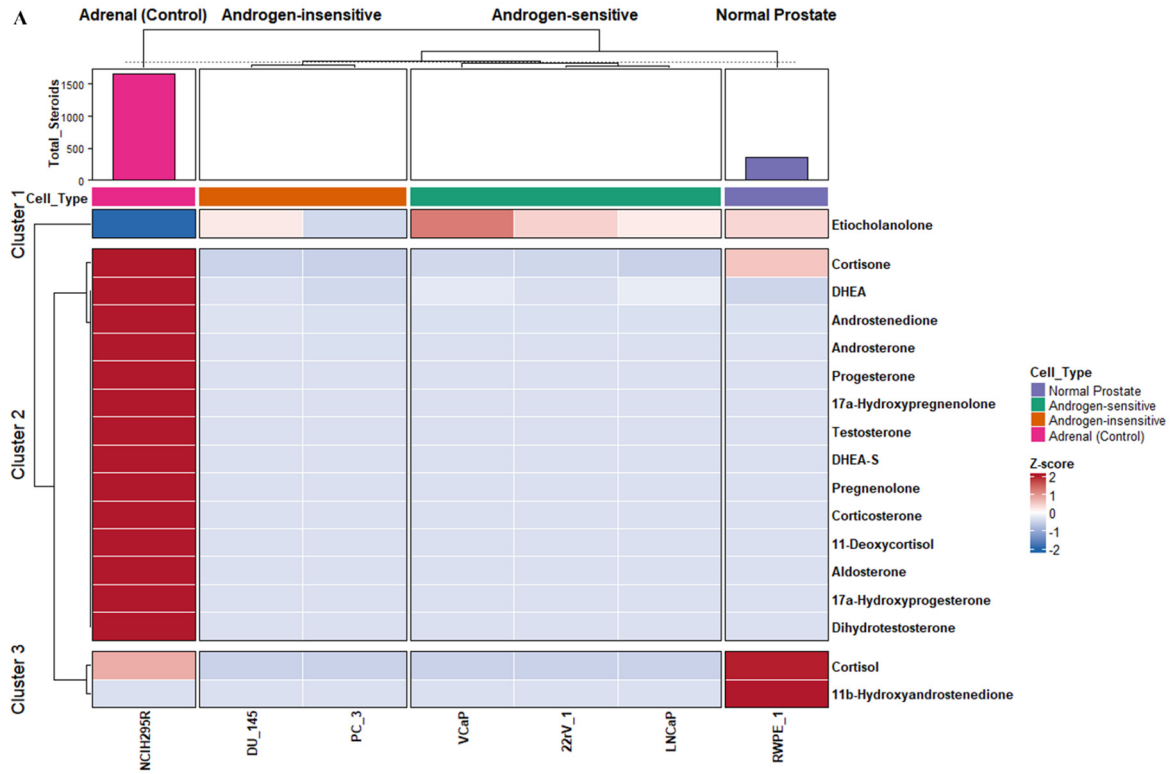

 doi:10.20944/preprints202604.0750.v1

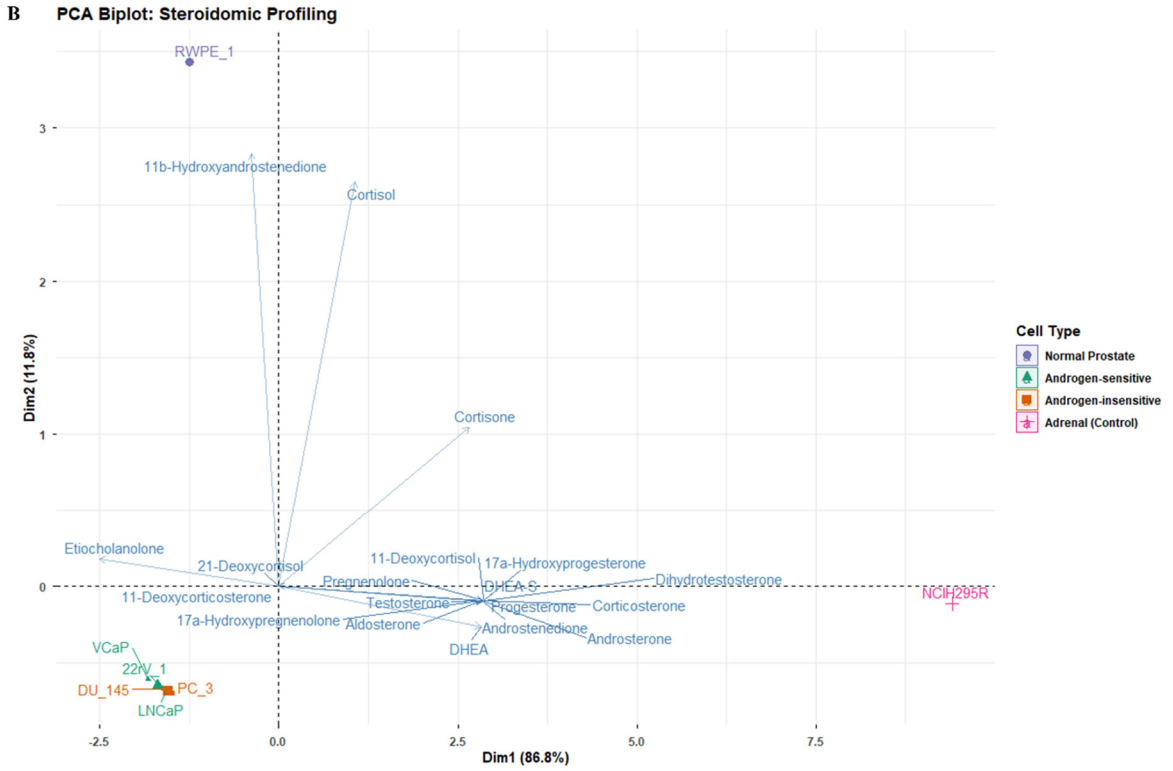

Figure 2. Steroid Profiling and Clustering of Prostate and H295R Cell Lines. A. Heatmap of log-transformed steroid levels across all prostate-derived and H295R cell lines cultured under androgen-depleted conditions. The heatmap shows distinct clustering patterns, with H295R cells forming a separate cluster due to their broad steroidogenic profile. Prostate cancer cell lines exhibit variable steroid profiles, with RWPE-1 cells producing minimal steroids. **B.** Principal Component Analysis (PCA) of steroid profiles. H295R cells cluster distinctly from prostate cancer lines, driven by higher steroidogenic output, highlighting the variability in steroid biosynthesis across cell models. NB: DU145 (DU_145), PC3 (PC_3) and RWPE-1 (RWPE_1).

3. Comparative Overlap of Prostate Cancer Cell Lines Reveals Shared Malignant Core and Androgen-Dependent Divergence

To delineate shared versus lineage-specific transcriptional programs across PCa models, we performed comparative overlap analyses among multiple androgen-sensitive and androgen-independent cell lines, using the non-malignant prostate epithelial line RWPE-1 as a reference. When all malignant prostate cell lines (VCaP, LNCaP, 22Rv1, DU145, and PC3) were examined together, a substantial core set of genes was shared across all models (Figure 3A–C). This central overlap indicates the existence of fundamental transcriptional programs characteristic of malignant prostate epithelium, independent of androgen receptor (AR) signaling status. These shared genes likely represent baseline tumor identity features that are maintained through progression and across diverse genetic backgrounds. Despite this conserved malignant core, each cell line also retained a sizable number of unique genes, reflecting pronounced inter-model heterogeneity. These non-overlapping gene sets likely correspond to context-specific adaptations that distinguish individual disease subtypes and stages represented by each model. To assess how malignant prostate cells diverge from non-malignant prostate epithelium, RWPE-1 was next compared with androgen-sensitive PCa lines (VCaP, LNCaP, and 22Rv1). Although a substantial intersection was observed, these cancer cell lines shared a distinct overlap absent in RWPE-1, consistent with transcriptional changes associated with malignant transformation in an androgen-responsive context. At the same time, the overlap with RWPE-1 suggests partial preservation of prostate epithelial lineage identity in AR-positive models, consistent with their more differentiated luminal-like state. In contrast, comparison of RWPE-1 with androgen-independent cell lines (PC3 and DU145) revealed a markedly reduced overlap. These castration-resistant models shared a substantial set of genes absent in RWPE-

 doi:10.20944/preprints202604.0750.v1

1, signifying transcriptional reprogramming events associated with androgen independence and more advanced disease states. The shared gene pool between PC3 and DU145 likely captures lineage plasticity, survival adaptations, and loss of epithelial specialization characteristic of late-stage prostate cancer. These comparative analyses demonstrate that prostate cancer cell lines maintain a conserved malignant core signature while diverging according to androgen dependence and disease progression. Androgen-sensitive models retain greater similarity to non-malignant epithelium, whereas androgen-independent cell lines exhibit pronounced transcriptional deviation, reflecting the acquisition of aggressive, AR-independent phenotypes.

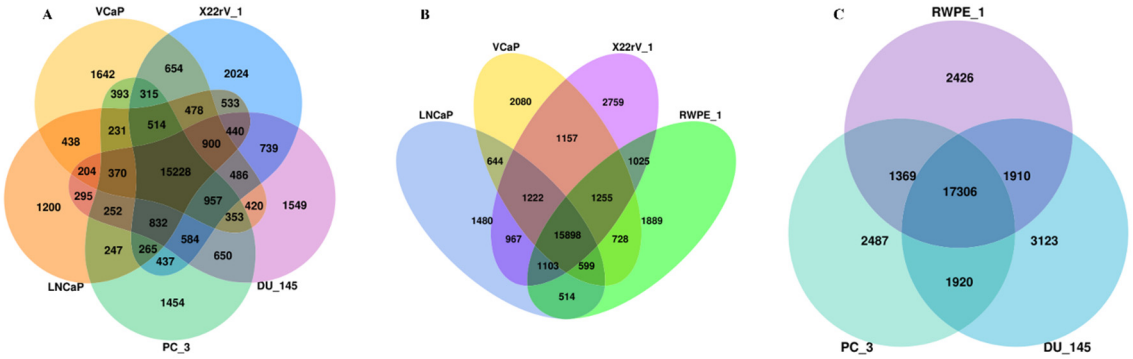

Figure 3. Comparative overlap analysis of prostate cancer cell lines based on androgen sensitivity. Venn diagrams illustrate shared and unique genes among prostate cancer cell lines and normal prostate epithelial cells. **(A)** Overlap of genes across prostate cancer cell lines (VCaP, LNCaP, 22Rv1, DU145, and PC3), excluding the normal prostate epithelial cell line RWPE-1, highlighting a conserved malignant core shared across all cancer models alongside cell line–specific signatures. **(B)** Comparison of RWPE-1 with androgen-sensitive prostate cancer cell lines (VCaP, LNCaP, and 22Rv1), showing both shared epithelial features and cancer-specific gene sets associated with androgen receptor–dependent tumorigenesis. **(C)** Comparison of RWPE-1 with androgen-independent prostate cancer cell lines (DU145 and PC3), demonstrating reduced overlap with normal prostate epithelium and increased transcriptional divergence characteristic of advanced, androgen-independent disease. Numbers indicate the total genes unique to or shared among the indicated cell lines. NB: DU145 (DU_145), PC3 (PC_3), 22Rv-1 (X22rV_1) and RWPE-1 (RWPE_1).

4. Gene Expression Clustering in Prostate Cancer Cell Lines

4.1. Differential Expression of Canonical Prostate Cancer Signaling Genes

The panel of prostate cancer–associated signaling genes demonstrated distinct expression signatures across the six cell lines, reflecting known molecular subtypes and pathway dependencies. Hierarchical clustering segregated the cell lines into discrete groups, indicating that each line harbors a characteristic signaling landscape. Notably, VCaP and LNCaP clustered more closely to one another, consistent with their androgen receptor (AR)-positive phenotypes, while PC3 and DU145 showed more divergent patterns aligned with AR-independent profiles. Genes associated with PI3K/AKT/mTOR signaling (PIK3CA, AKT1-3, MTOR) exhibited heterogeneous regulation across lines. VCaP demonstrated higher expression of *AKT1/2* and upstream receptor-linked components, whereas PC3 exhibited comparatively reduced expression of multiple AKT pathway members. Conversely, DU145 showed increased expression of *KLK3* and *ERG*, reflecting FGF- and ERG-driven oncogenic programs. AR-axis genes such as *AR*, *NKX3-1*, and *KLK3* were enriched in LNCaP and VCaP, reaffirming their androgen-dependent phenotype, whereas these genes were notably depleted in PC3 and DU145, consistent with their androgen-independent and neuroendocrine-leaning characteristics. Tumor suppressor genes, including RB1, PTEN, and TP53, displayed variable suppression among androgen-independent lines. PC3 exhibited lower *RB1* and *PTEN* levels, aligning

 doi:10.20944/preprints202604.0750.v1

with the known loss-of-function events frequently observed in late-stage CRPC. Our data confirms that each cell line recapitulates distinct molecular subsets of prostate cancer progression and therapeutic response.

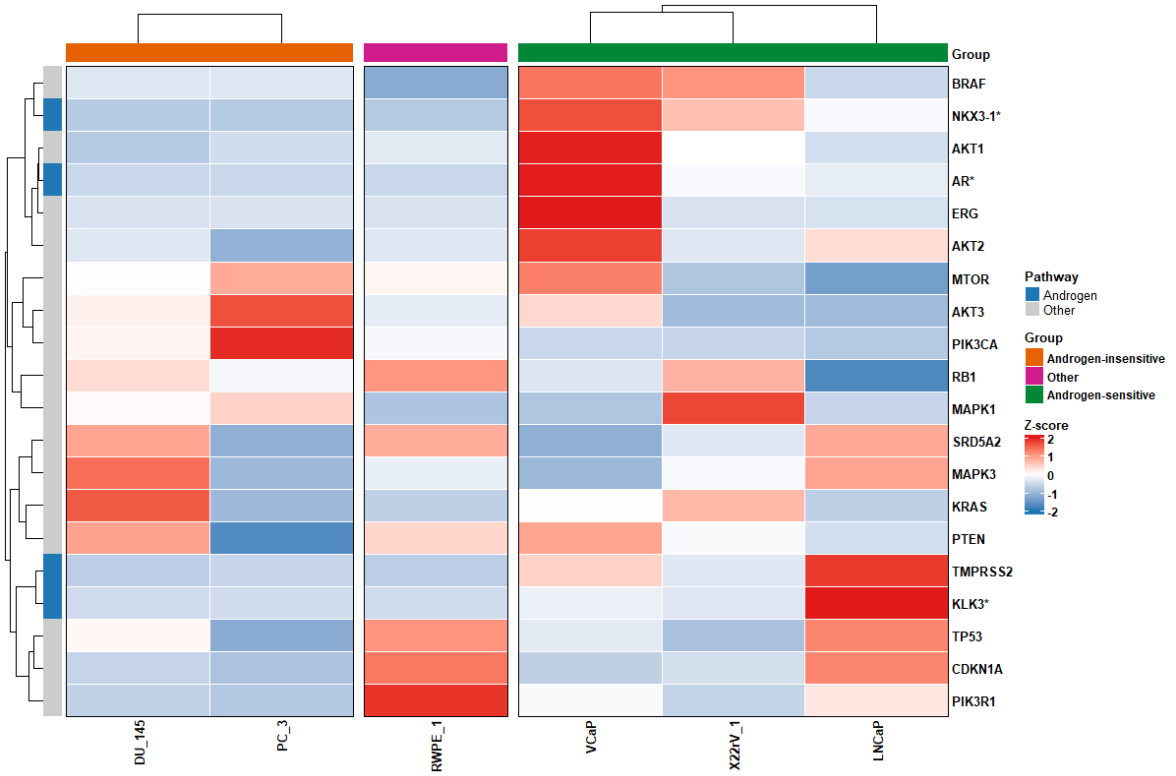

Figure 4. Heatmap of prostate cancer-associated signaling gene expression across cell lines. Hierarchical clustering of gene expression values is shown for six prostate cell lines (PC3, VCaP, RWPE-1, DU145, LNCaP, and 22rV-1). Expression values are scaled by Z-score, with red indicating upregulation and blue indicating downregulation. Clustering highlights distinct molecular signatures and pathway activation states among androgen-dependent and androgen-independent prostate cancer models. NB: DU145 (DU_145), PC3 (PC_3), 22Rv-1 (X22rV_1) and RWPE-1 (RWPE_1).

4.2. Steroidogenic Pathway Gene Expression Across Cell Lines

Analysis of steroidogenic and cholesterol-handling genes further stratified the prostate cancer models by their capacity to synthesize or utilize intratumoral androgens. Hierarchical clustering revealed that LNCaP and VCaP showed the highest expression of genes involved in androgen biosynthesis and metabolism, including cytochrome P450 family members (CYP17A1, CYP11A1, CYP19A1), oxidoreductases (HSD17B family), and cholesterol trafficking genes (STAR, TSPO, SCARB1). This steroidogenic enrichment supports the concept that AR-positive prostate cancer can generate intracrine androgen pools that sustain AR signaling under castration pressure. In contrast, androgen-independent lines such as PC3 and DU145 showed markedly reduced expression across multiple enzymatic nodes of the steroidogenic cascade, suggesting limited capacity for de novo androgen synthesis. Interestingly, several intermediate metabolic enzymes (e.g., *HSD3B1/2 and the AKR1C family*) remained expressed at moderate levels in DU145, indicating partial retention of steroid metabolism despite the absence of AR signaling. Cholesterol-importing genes, such as SCARB1, exhibited cell line-specific patterns, suggesting differing reliance on exogenous lipids for membrane synthesis and on steroid precursor pools. These expression profiles reinforce established phenotypes: AR-dependent tumors retain biosynthetic competence for steroid hormone production, whereas AR-independent CRPC tends to circumvent reliance on the AR axis in favour of alternative oncogenic pathways.

 doi:10.20944/preprints202604.0750.v1

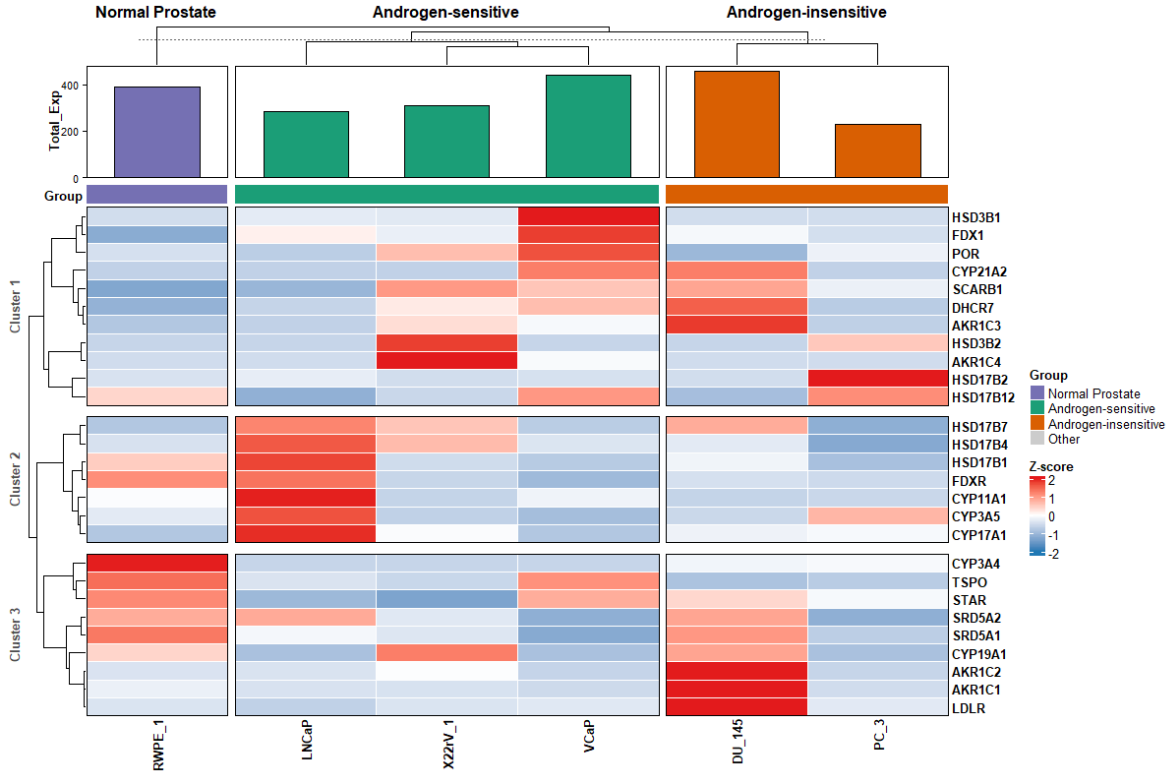

Figure 5. Heatmap of steroidogenic and cholesterol metabolism gene expression across cell lines. Expression of genes involved in steroid biosynthesis, conversion, and cholesterol transport is displayed across six prostate cell lines. Hierarchical clustering segregates AR-positive lines (VCaP, LNCaP) as enriched for steroidogenic enzymes, while androgen-independent lines exhibit attenuated steroidogenic capacity. Expression values are Z-score-scaled, with red indicating higher expression and blue indicating lower expression. NB: DU145 (DU_145), PC3 (PC_3), 22Rv-1 (X22rV_1) and RWPE-1 (RWPE_1).

4.3. Differential Androgen and Ferroptosis Gene Expression Signatures Distinguish Androgen-Sensitive and Androgen-Insensitive Prostate Cancer Cell Lines

Ferroptosis is a regulated, iron-dependent form of non-apoptotic cell death characterized by lipid peroxidation and oxidative membrane damage. Unlike apoptosis, ferroptosis is driven by dysregulated redox balance and impaired lipid peroxide detoxification, processes tightly controlled by regulators such as GPX4, SLC7A11, and iron-handling proteins. Increasing evidence suggests that ferroptosis plays an important role in advanced prostate cancer, particularly in CRPC, where tumors adapt to androgen deprivation through metabolic and redox reprogramming [34,35]. As canonical AR signaling becomes diminished or bypassed in CRPC, alterations in lipid metabolism and oxidative stress pathways create new vulnerabilities that can potentially be therapeutically exploited.

To further characterize molecular differences between androgen-sensitive (LNCaP, VCaP, and 22Rv1) and androgen-insensitive (DU145 and PC3) prostate cancer cell lines, we performed differential gene expression and pathway-focused analyses integrating androgen signaling and ferroptosis-related genes (*Figure 6*). The volcano plot (Figure 6A) shows a clear transcriptional divergence between the two groups. Androgen-sensitive cell lines exhibit significant upregulation of canonical AR pathway genes, including AR, KLK2, KLK3, NKX3-1, FOXA1, TMPRSS2, and ALOX15. The strong enrichment of AR and its downstream targets showed that intact androgen signaling occurs in LNCaP, VCaP, and 22Rv1 cells. This transcriptional profile reflects androgen dependence and supports the continued clinical relevance of AR-targeted therapies in CRPC.

Compared with androgen-insensitive cells, DU145 and PC3 cells display marked downregulation of AR and AR-responsive genes, consistent with loss of canonical AR signaling. This

 doi:10.20944/preprints202604.0750.v1

molecular pattern mirrors features observed in CRPC, where tumor growth becomes less dependent on classical androgen signaling. Boxplot analysis (*Figure 6D*) further highlights the pronounced elevation of AR expression in androgen-sensitive lines compared with minimal expression in androgen-insensitive and NCIH295R cells of adrenal origin and in RWPE-1, adapted from normal prostate epithelial cells, reinforcing AR signaling as the dominant distinguishing feature between these phenotypes.

Beyond androgen signaling, ferroptosis-related genes also show differential expression patterns (*Figures 6B-C*). Several ferroptosis regulators, including GPX4, ACSL4, TFRC, SLC7A11, HMOX1, and FTH1, exhibit distinct shifts between the three groups. The androgen-sensitive cells show higher expression of certain ferroptosis-associated genes such as ALOX15 and GPX4, suggesting an interaction between androgen signaling and lipid peroxidation pathways. Meanwhile, androgen-insensitive lines exhibit altered expression of iron-handling and oxidative stress regulators, including TFRC and HMOX1, suggesting a rewiring of redox homeostasis.

The heatmap (*Figure 6B*) illustrates clustering of androgen-sensitive cells driven primarily by strong AR-axis activation, while androgen-insensitive samples cluster separately, characterized by diminished AR pathway activity and relative enrichment of selected ferroptosis-related genes. The pathway-focused scatter analysis (*Figure 6C*) further shows that androgen pathway genes consistently exhibit positive $\log_2$ fold changes in sensitive cells, whereas ferroptosis genes display more heterogeneous regulation, suggesting a complex relationship between androgen responsiveness and ferroptotic vulnerability.

Our results show a coordinated suppression of canonical AR signaling, along with altered ferroptosis-associated gene expression, in androgen-insensitive cell lines. This integrated transcriptional reprogramming depicts the biological transition from androgen dependence to androgen independence and suggests that ferroptosis regulation represents an additional adaptive mechanism in advanced prostate cancer. Therapeutically, while AR pathway inhibition remains central for androgen-sensitive disease, modulation of ferroptosis regulators, either to induce ferroptotic cell death or to exploit altered redox states, provides complementary strategies in androgen-insensitive or CRPC.

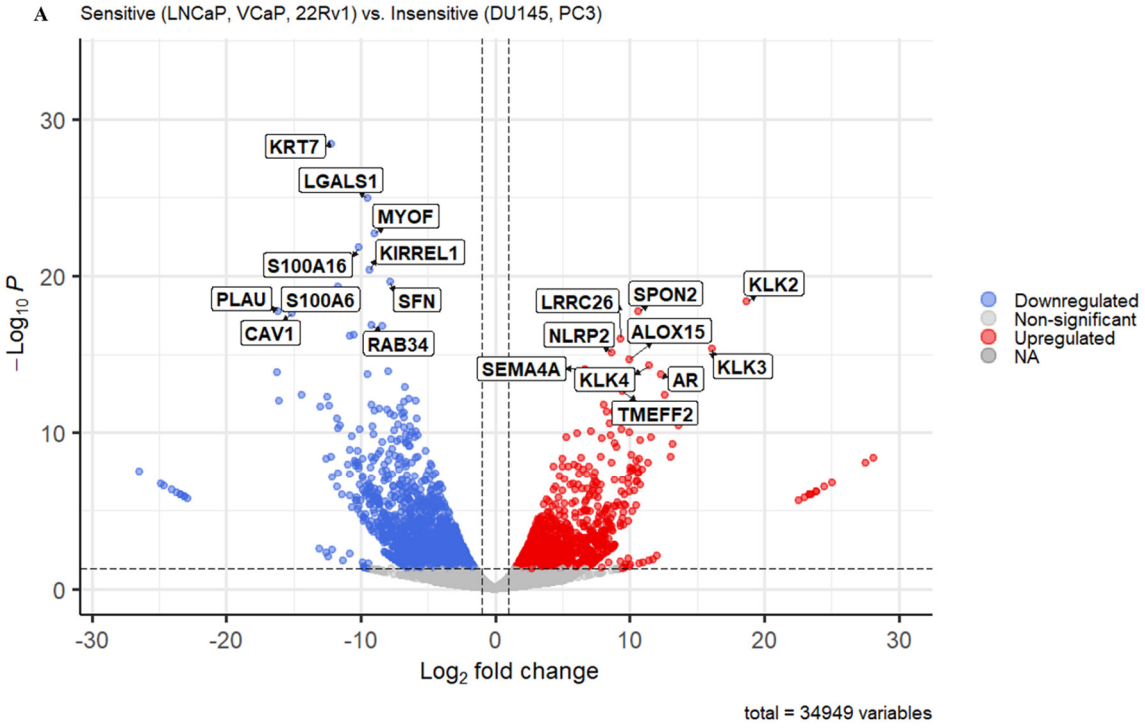

 doi:10.20944/preprints202604.0750.v1

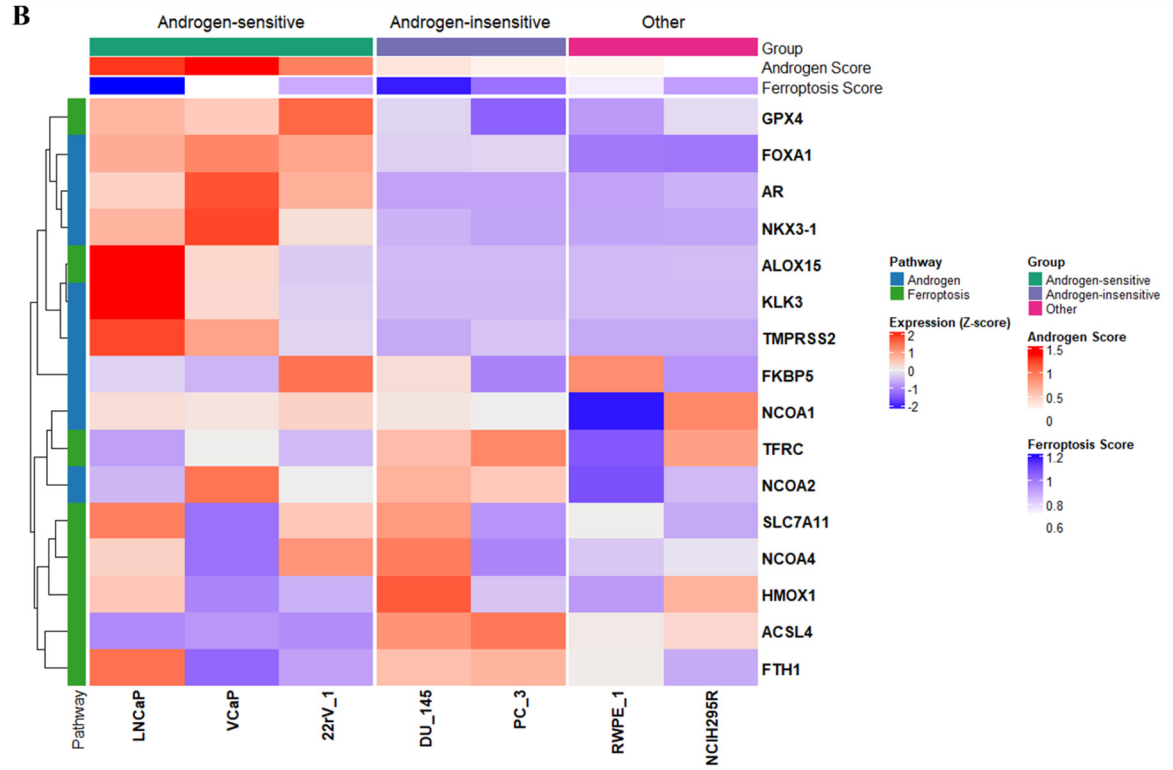

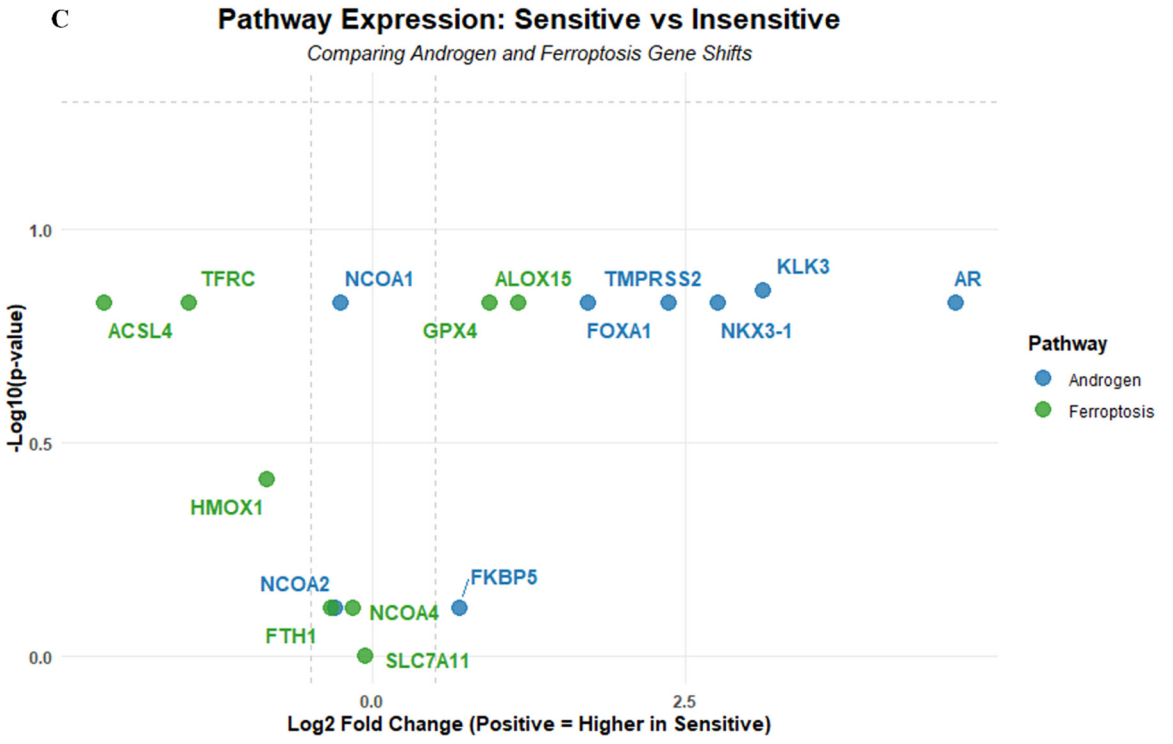

 doi:10.20944/preprints202604.0750.v1

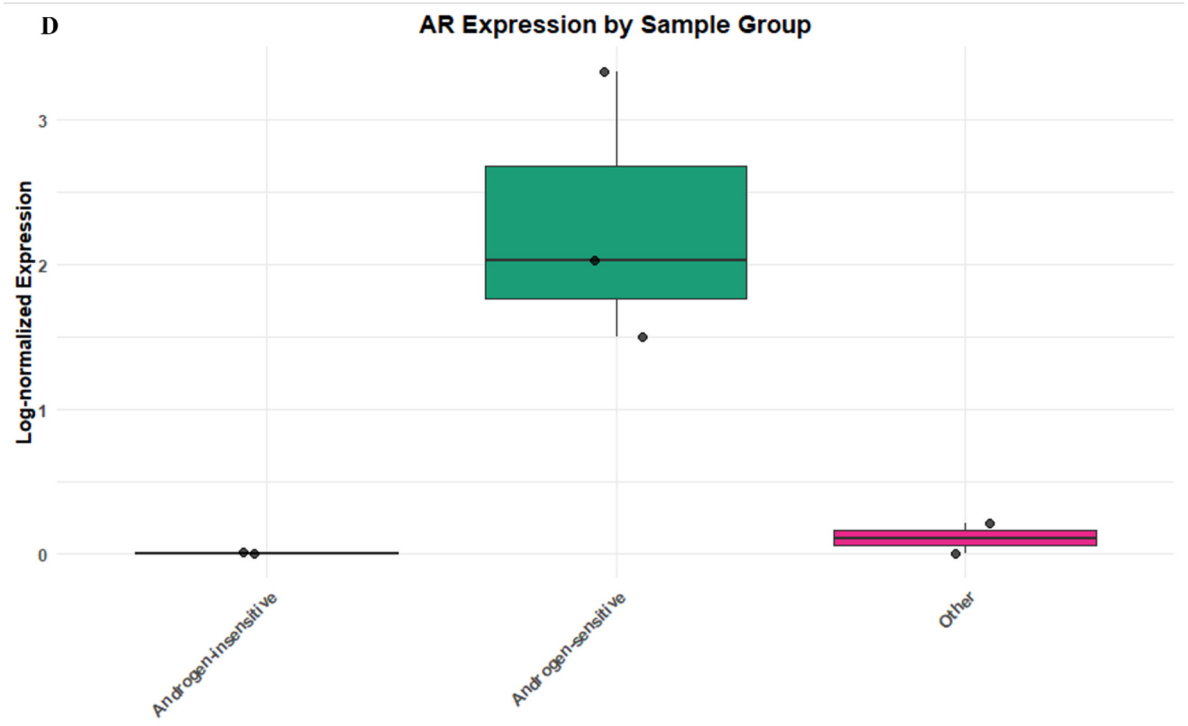

Figure 6. The Integrated analysis of androgen and ferroptosis gene expression in androgen-sensitive and androgen-insensitive prostate cancer cell lines. (A) Volcano plot of differential gene expression comparing androgen-sensitive (LNCaP, VCaP, 22Rv1) versus androgen-insensitive (DU145, PC3) cell lines. Red dots indicate significantly upregulated genes in sensitive lines; blue dots indicate significantly downregulated genes; grey dots represent non-significant genes. Selected androgen and ferroptosis-related genes are labelled. (B) Heatmap of scaled expression (Z-score) of androgen pathway and ferroptosis-related genes across all cell lines. Samples cluster according to androgen sensitivity status, with strong enrichment of AR-axis genes in sensitive lines. (C) Pathway-focused scatter plot showing $\log_2$ fold change (sensitive vs insensitive) versus $-\log_{10}$(p-value) for androgen (blue) and ferroptosis (green) genes, highlighting coordinated upregulation of androgen signaling and heterogeneous ferroptosis gene shifts. (D) Boxplot of log-normalized AR expression across sample groups, demonstrating significantly higher AR expression in androgen-sensitive cell lines compared with androgen-insensitive and other groups. NB: DU145 (DU_145), PC3 (PC_3), 22Rv-1 (X22rV_1) and RWPE-1 (RWPE_1).

4.4. Principal Component Analysis of Steroidogenic Gene Expression

PCA was performed to assess transcriptional heterogeneity in steroidogenic pathway genes across prostate cancer cell lines. The first three principal components accounted for a substantial proportion of the total variance and effectively discriminated against cell models. The 3-dimensional PCA projection revealed clear AR-positive versus AR-negative lines, driven primarily by genes associated with cholesterol transport, steroid biosynthesis, and androgen metabolism. AR-positive cell lines clustered more closely together, indicating conserved activation of steroidogenic pathways, while AR-negative models occupied distinct positions within the PCA space, reflecting divergent metabolic and endocrine profiles. Our data support the presence of lineage-specific steroidogenic programming in prostate cancer and are consistent with known differences in androgen dependence between models.

 doi:10.20944/preprints202604.0750.v1

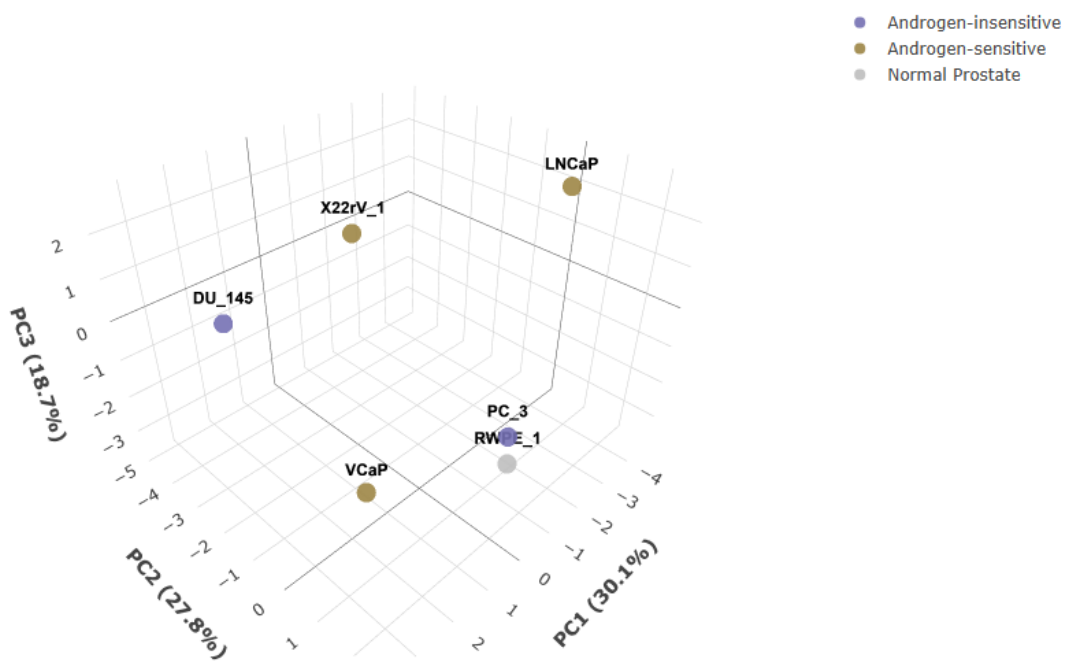

Figure 7. 3-Dimensional principal component analysis (PCA) of steroidogenic gene expression across prostate cancer cell lines. Log_1-transformed expression values of curated steroidogenic pathway genes were subjected to PCA. PC1, PC2, and PC3 accounted for the major sources of variance and discriminated against AR-positive from AR-negative prostate cancer models. Clustering patterns indicate differential activation of steroid biosynthesis, cholesterol metabolism, and androgen signaling pathways between cell line subtypes. NB: DU145 (DU_145), PC3 (PC_3), 22Rv-1 (X22rV_1) and RWPE-1 (RWPE_1).

5. Functional Enrichment Analysis of Differentially Expressed Prostate Cancer-Associated Genes

To elucidate the functional architecture and clinical relevance of the identified gene set, we performed a multi-platform enrichment analysis encompassing KEGG, Gene Ontology (GO), Reactome, Disease Ontology (DO), and DisGeNET (Figure 8). KEGG and Reactome pathway analyses revealed a significant convergence on core oncogenic signaling modules, most notably the PI3K/AKT, ErbB, and FGFR1/FGFR3 signaling axes, which are established drivers of growth and pro-survival networks in CRPC. These results were confirmed by GO functional annotation, which demonstrated significant enrichment in molecular functions related to steroid and nuclear hormone receptor binding, as well as biological processes involving androgen biosynthetic regulation and intrinsic apoptotic signaling. Notably, the enrichment of cellular senescence and platinum drug resistance pathways suggests a pivotal role for these genes in cellular adaptation to therapeutic stress. This molecular landscape was further reflected in DO and DisGeNET analyses, which identified strong associations with hormone-dependent malignancies and hereditary neoplastic syndromes, particularly those linked to DNA repair deficiencies such as *BRCA1/2*-linked pathways. Our results show the gene set at a critical intersection of receptor tyrosine kinase signaling, steroid hormone metabolism, and genomic maintenance, highlighting a conserved oncogenic framework that drives tumor progression and therapy resistance across multiple malignant contexts.

 doi:10.20944/preprints202604.0750.v1

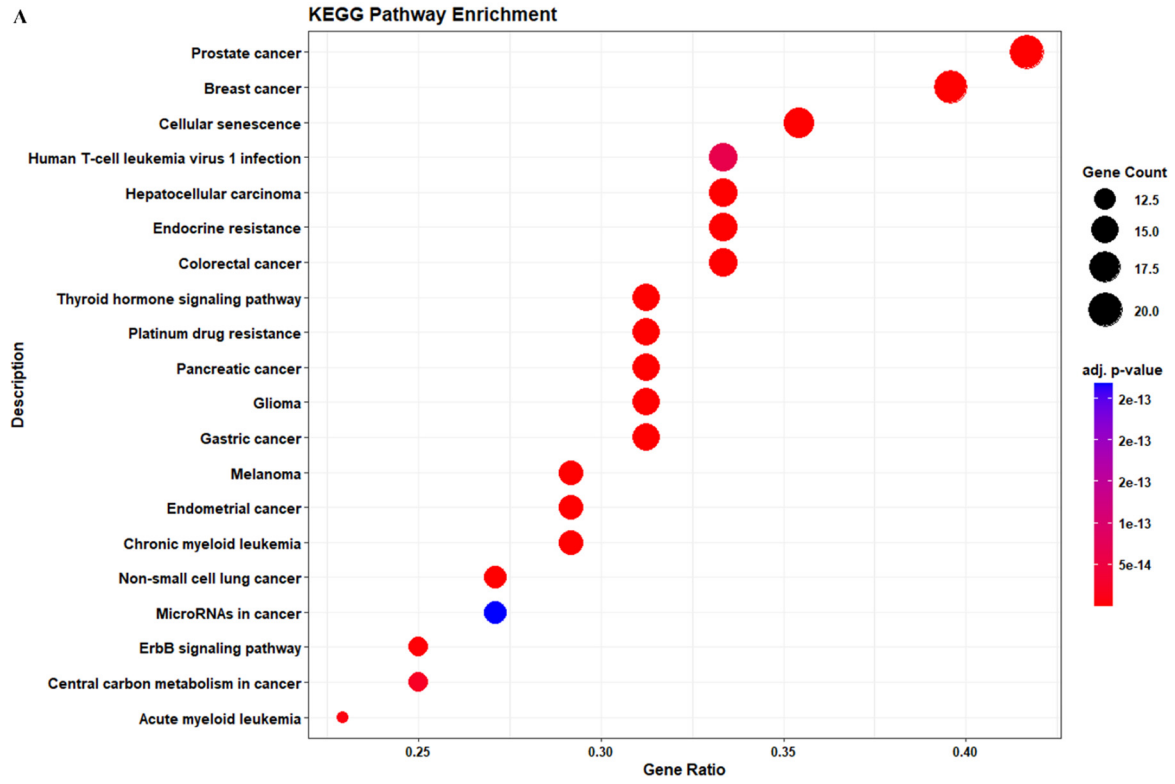

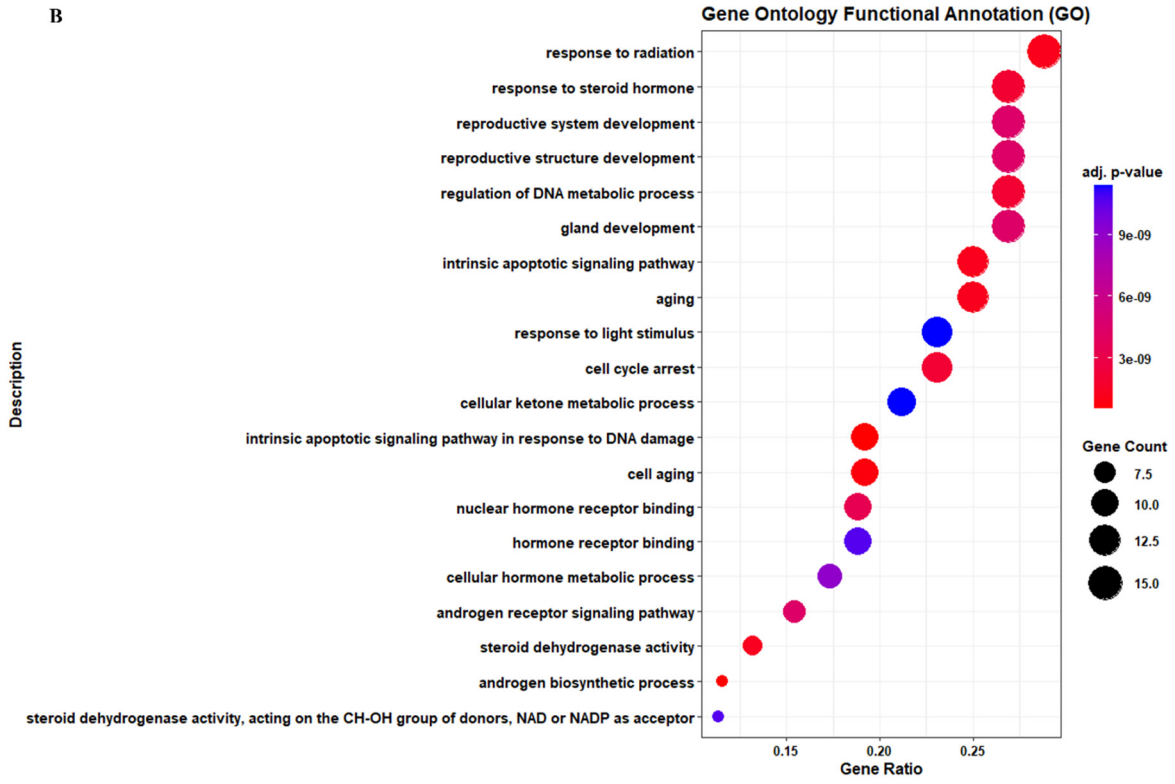

 doi:10.20944/preprints202604.0750.v1

C

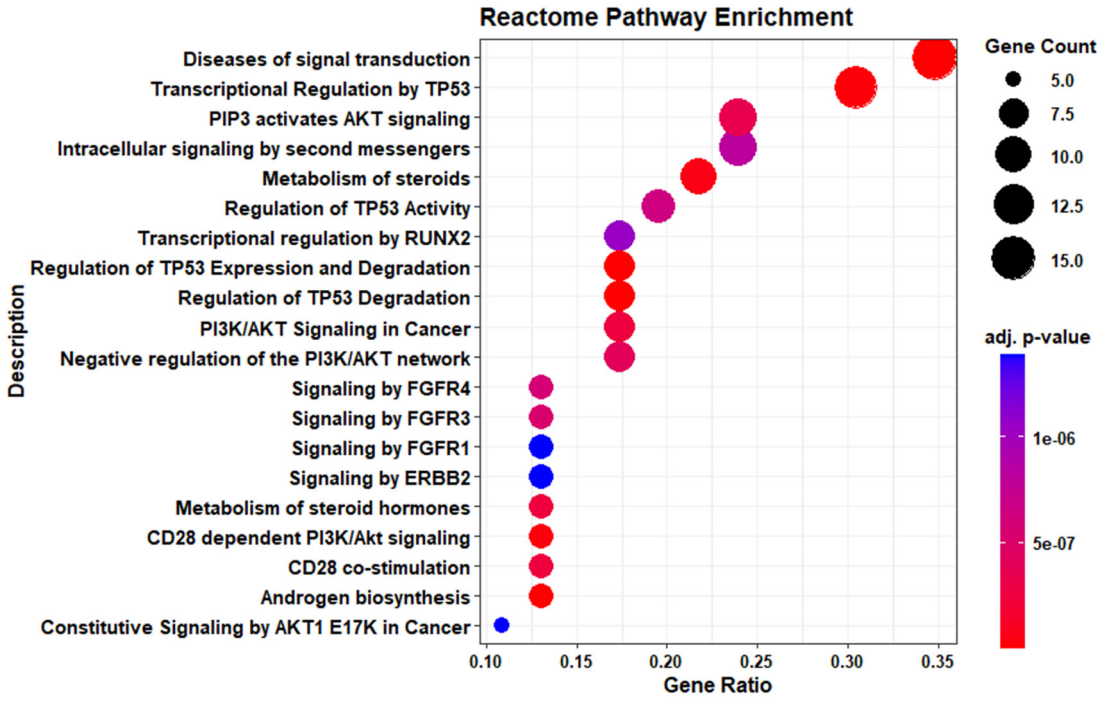

D

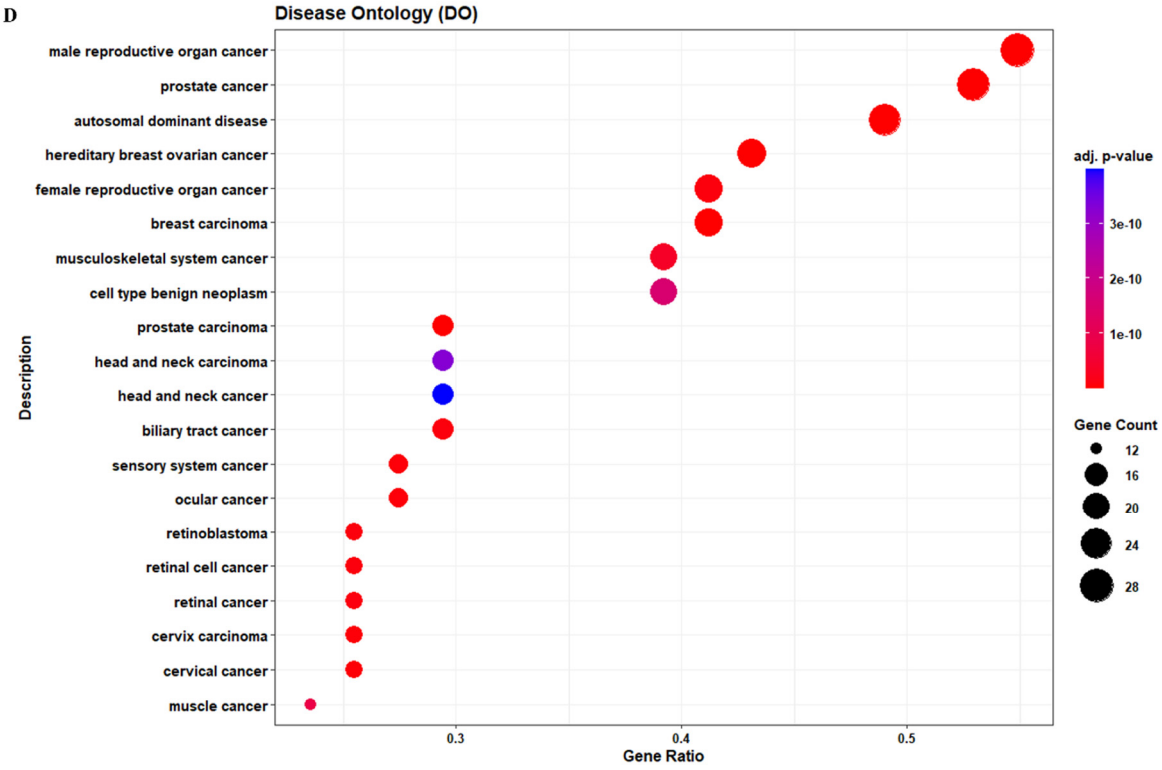

 doi:10.20944/preprints202604.0750.v1

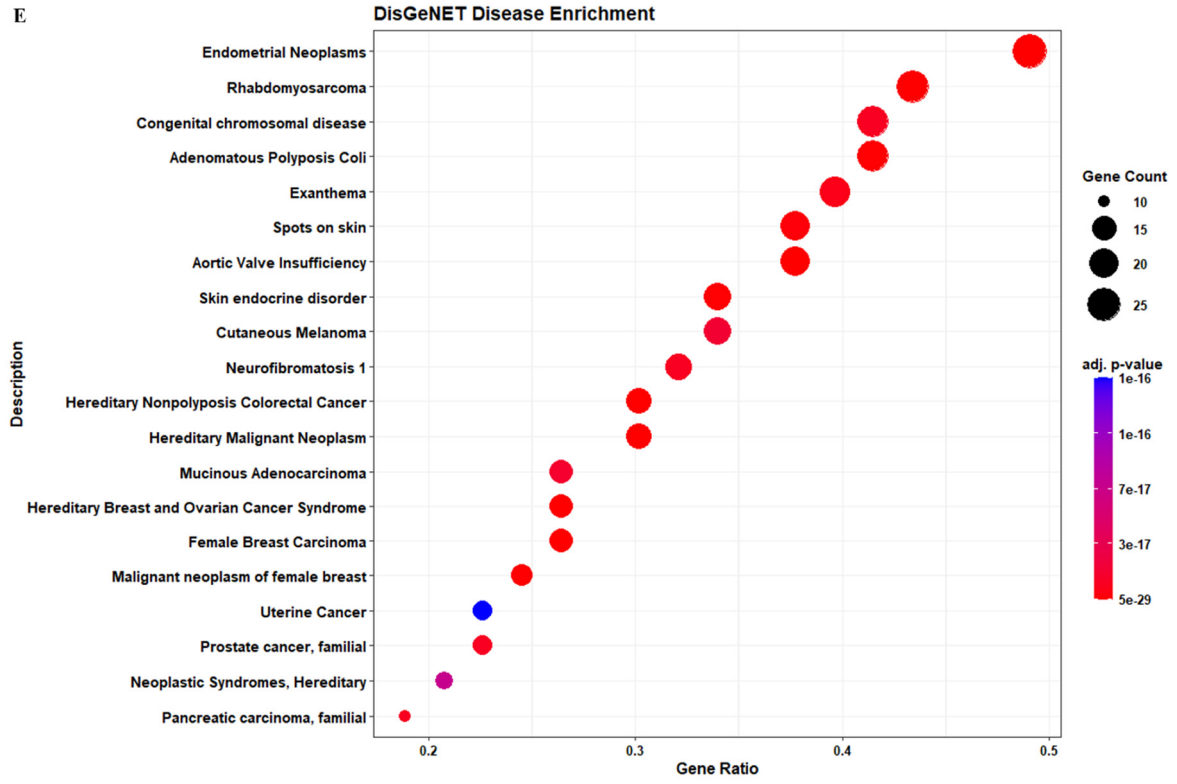

Figure 8. The comprehensive bioinformatics characterization of the target gene set across five independent functional enrichment databases. (A) KEGG Pathway Enrichment and (C) Reactome Pathway Enrichment highlight the involvement of growth factor-mediated oncogenic signaling and steroid metabolism. (B) Gene Ontology (GO) Functional Annotation categorizes genes into Biological Process, Molecular Function, and Cellular Component, with emphasis on androgen receptor binding and metabolic regulation. (D) Disease Ontology (DO) and (E) DisGeNET Enrichment illustrate the clinical phenotype landscape, showing associations with hormone-dependent cancers and hereditary syndromes. For all panels, the x-axis indicates the Gene Ratio, bubble size represents Gene Count, and the color gradient corresponds to the statistical significance (adjusted p-value).

6.0. The Interplay Between AR Regulatory Flux and Metabolic Reprogramming in PRAD

6.1. Distinct Transcriptomic and Bioenergetic Profiles of AR-High PRAD

To transition from *in vitro* metabolic observations to clinical phenotypes, we characterized the transcriptomic landscape of 818 PRAD samples, stratified by AR transcript abundance (Figure 9A). GSEA revealed a robust activation of the Androgen Response hallmark in the AR-High cohort (*NES = 1.61, adj. p < 0.0001; Figure 1C*). Beyond classical AR signaling, the AR-High phenotype was defined by a coordinated bioenergetic program, with significant enrichment in Oxidative Phosphorylation, Fatty Acid Metabolism, and MTORC1 Signaling (Figure 9B, D). Conversely, the AR-High group showed a marked suppression of the EMT and Angiogenesis hallmarks, suggesting a more differentiated, albeit metabolically hyperactive, state compared to AR-Low tumors (Figure 9B). Differential expression analysis confirms these details, showing significant upregulation of core signaling nodes, including *PIK3CA* (*Log2FC = 0.90, p < 0.001*) and *mTOR* (*Log2FC = 0.75, p < 0.001*). Also, a concomitant increase in *PTEN* mRNA (*Log2FC = 0.38, p < 0.001*) was observed, potentially reflecting a compensatory feedback loop. Moreover, the AR-High group exhibited a shift in ferroptosis-related genes, including an upregulation of *SLC7A11* (*Log2FC = 0.52, p <0.001*) and *ACSL4* (*Log2FC = 0.37, p < 0.001*), while *GPX4* was significantly downregulated (*Log2FC = -0.34, p < 0.001*), highlighting a distinct vulnerability to lipid peroxidation.

 doi:10.20944/preprints202604.0750.v1

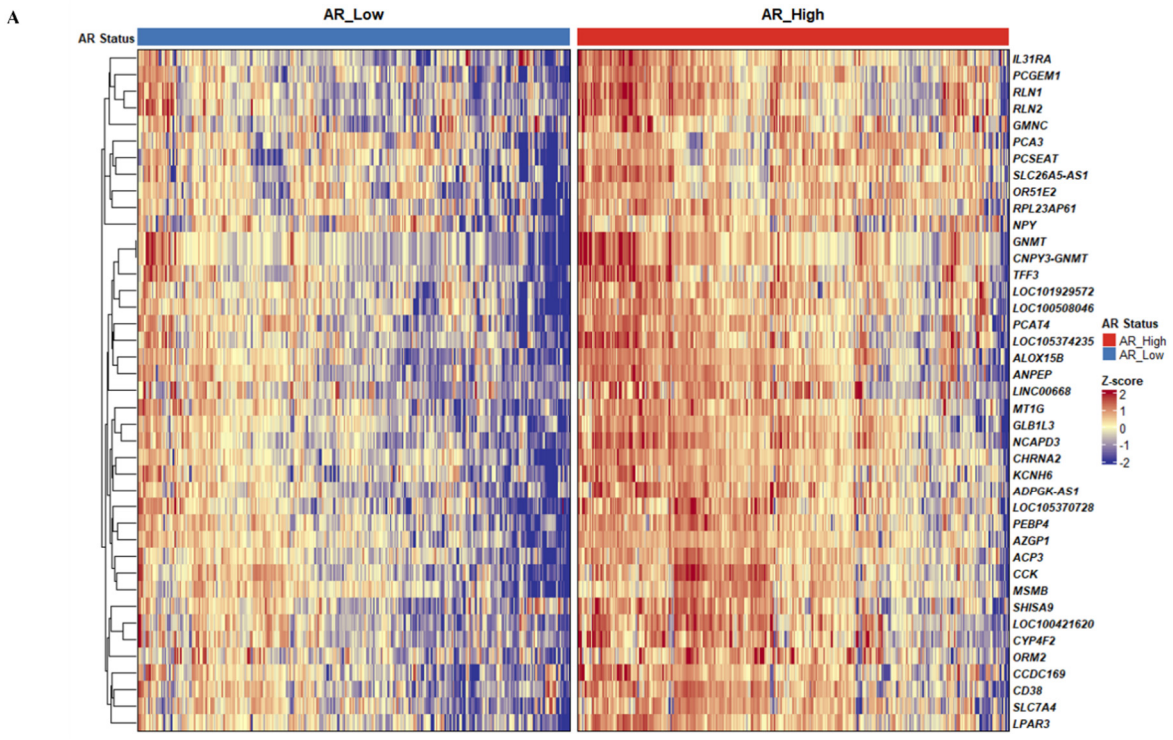

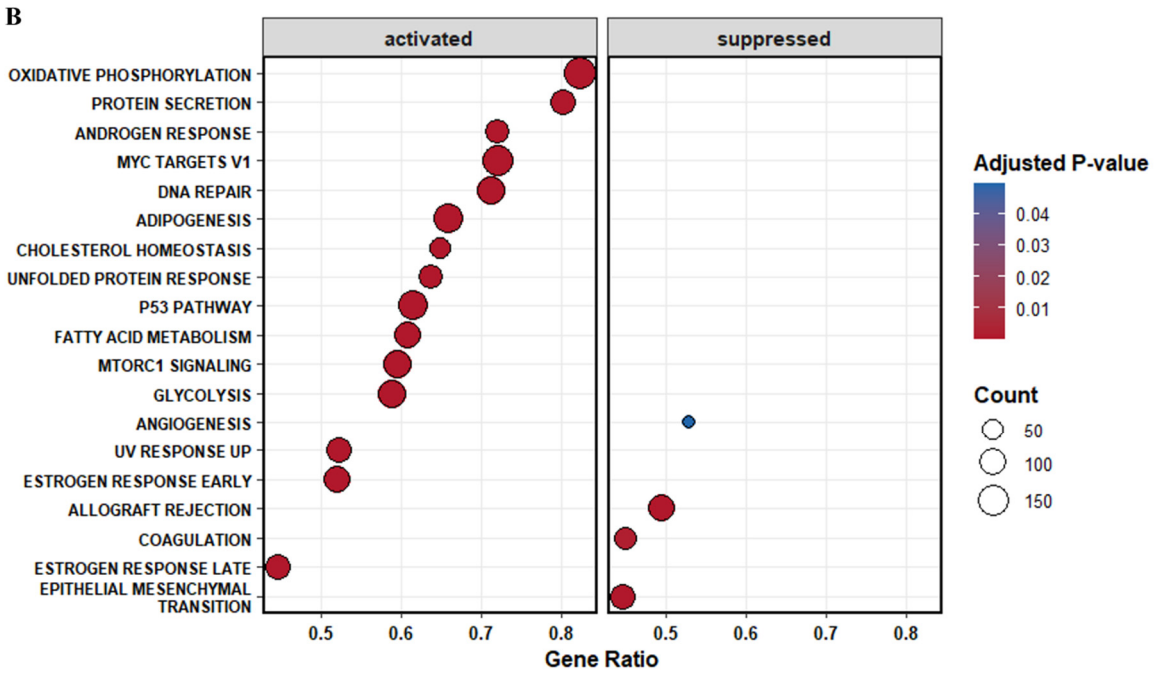

 doi:10.20944/preprints202604.0750.v1

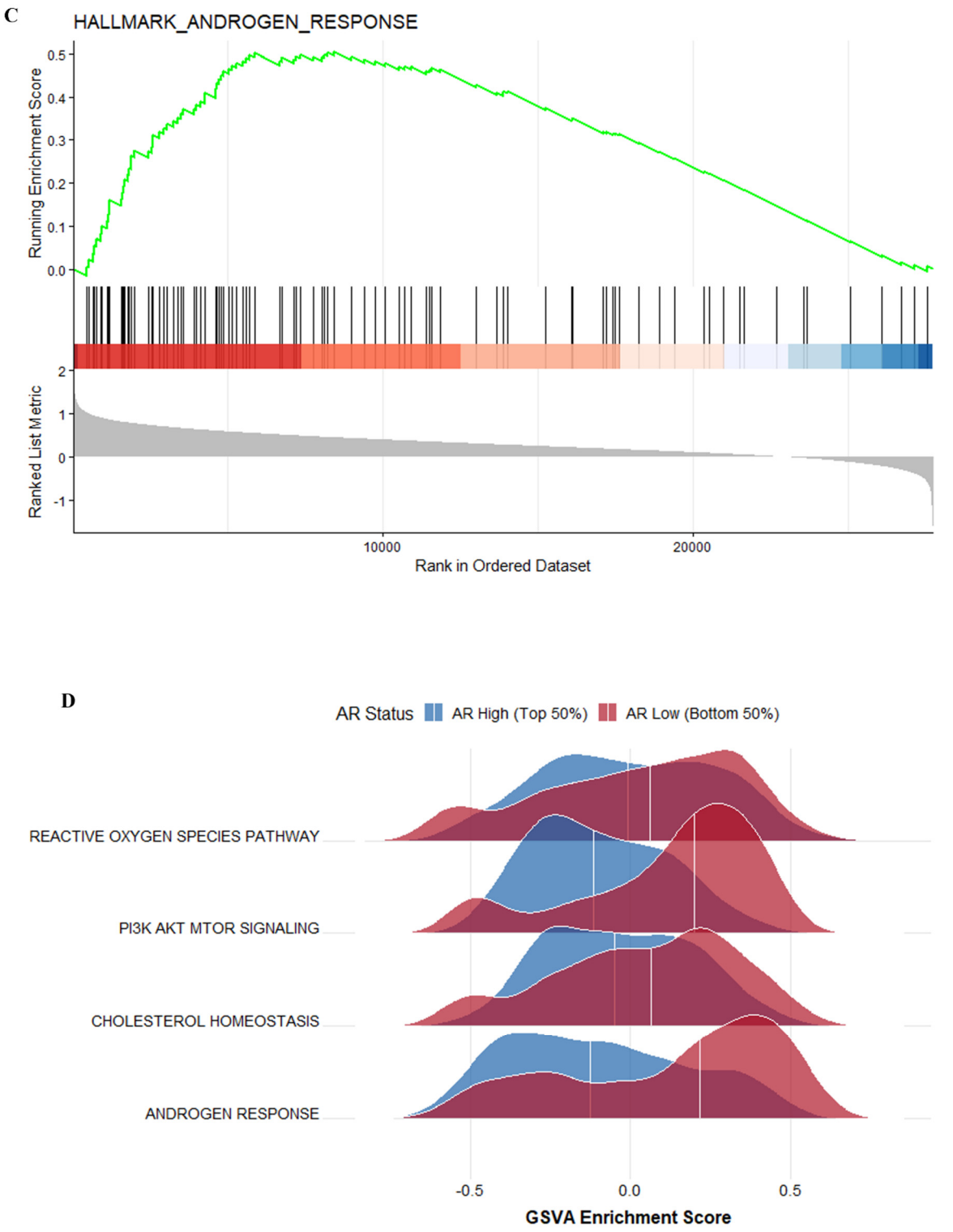

Figure 9. (A) Heatmap depicting the top differentially expressed genes between AR-Low and AR-High patient cohorts. (B) Dot plot of GSEA Hallmark pathways significantly activated (e.g., Oxidative Phosphorylation, MTORC1 Signaling) or suppressed (e.g., EMT, Angiogenesis) in AR-High tumors. Bubble size represents gene count; color indicates adjusted *p*-value. (C) GSEA enrichment plot for the Androgen Response hallmark (NES = 1.61, adj. $p < 0.0001$). (D) Ridge plots illustrating the distribution of enrichment scores for representative metabolic and signaling hallmarks across the AR-stratified cohorts.

 doi:10.20944/preprints202604.0750.v1

6.2. Molecular Stratification and Transcriptomic Characterization of AR Signaling States in Prostate Cancer

To characterize the molecular divergence associated with AR signaling in prostate cancer, we stratified our cohort into AR-high and AR-low phenotypes based on their transcriptomic profiles (Figure 10A). Global pathway analysis via GSVA revealed that AR-high tumors were defined by robust activation of canonical androgen response and oxidative phosphorylation pathways. In contrast, the AR-low subgroup exhibited significant enrichment in developmental and aggressive signaling programs, including Wnt/β-catenin, Notch, and EMT, suggesting a transition toward a more primitive, undifferentiated state (Figure 10A). Multidimensional mapping through UMAP further demonstrated the functional intersection between androgen signaling and metabolic reprogramming, specifically identifying a cluster of genes associated with ferroptosis and PI3K signaling that bridges these distinct phenotypes (Figure 10B). This was corroborated by targeted expression profiling, which showed that AR-high tumors maintained high levels of classical markers such as KLK3 and TMPRSS2, whereas AR-low tumors displayed a heterogeneous yet distinct shift in ferroptosis-regulating genes, including GPX4 and SLC7A11 (Figure 10C). Finally, we assessed the relationship between AR signaling and cellular plasticity. Although a statistically significant positive correlation was observed between inferred AR activity and the Plasticity/NEPC score ($R = 0.078$, $p = 0.025$), the broad distribution of AR-low samples suggests that while reduced AR signaling is a hallmark of lineage plasticity, additional epigenetic or stochastic factors likely drive the complete neuroendocrine transdifferentiating process (Figure 10D).

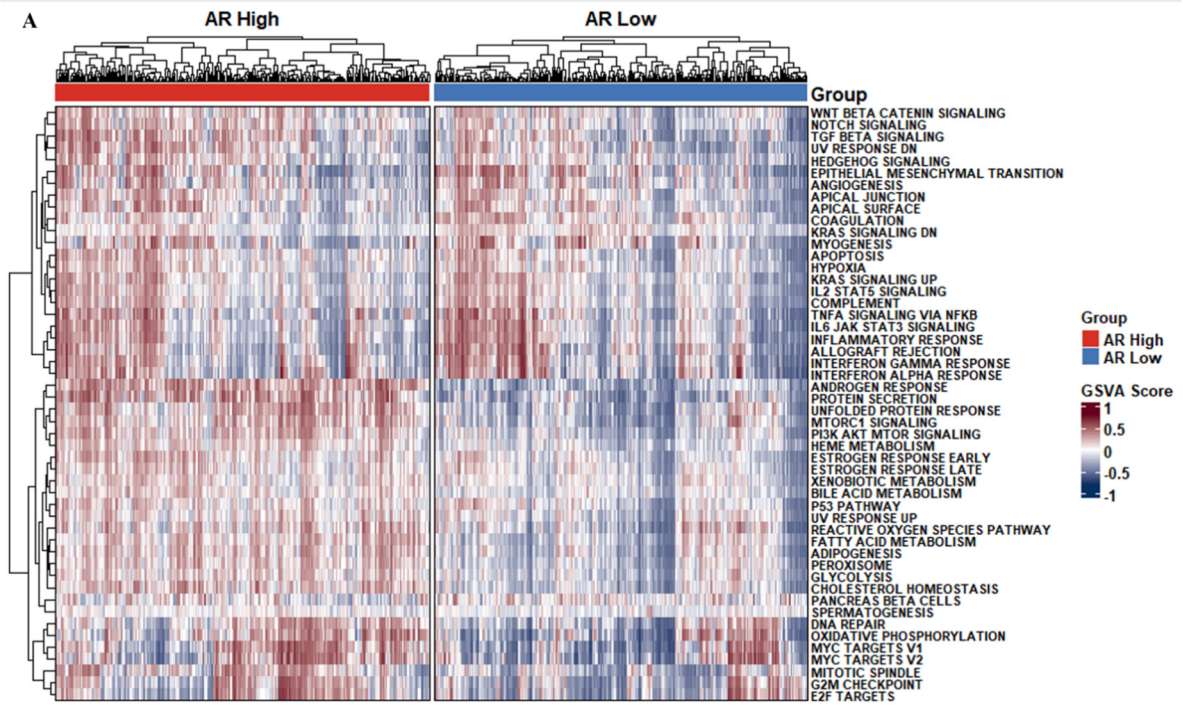

 doi:10.20944/preprints202604.0750.v1

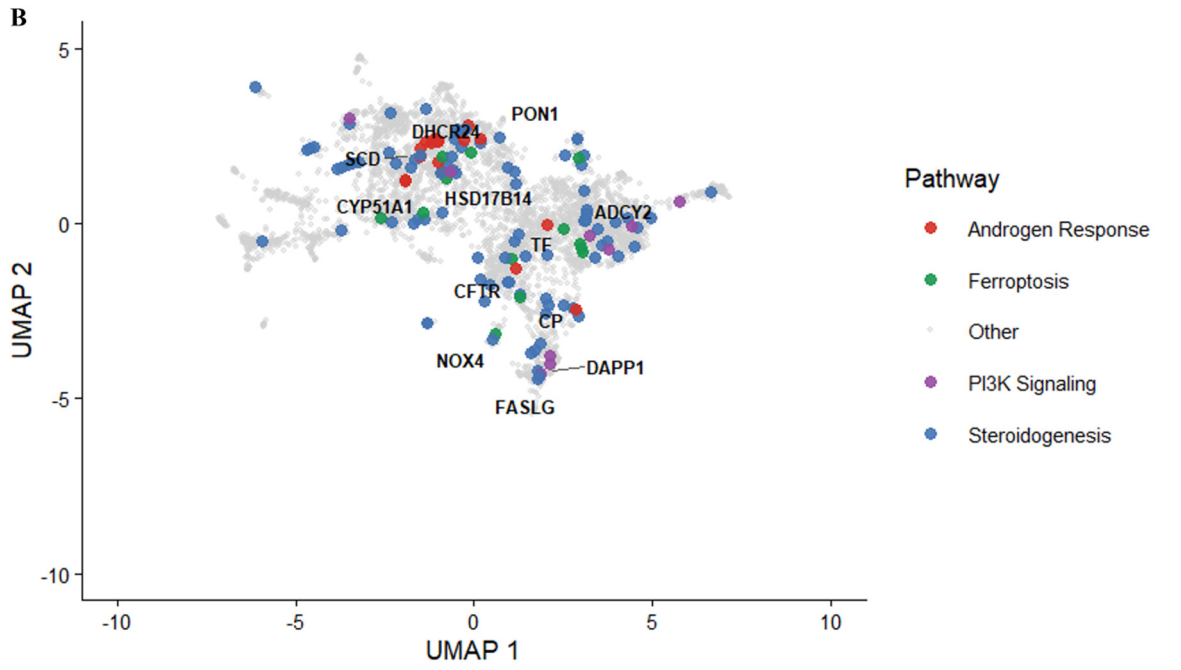

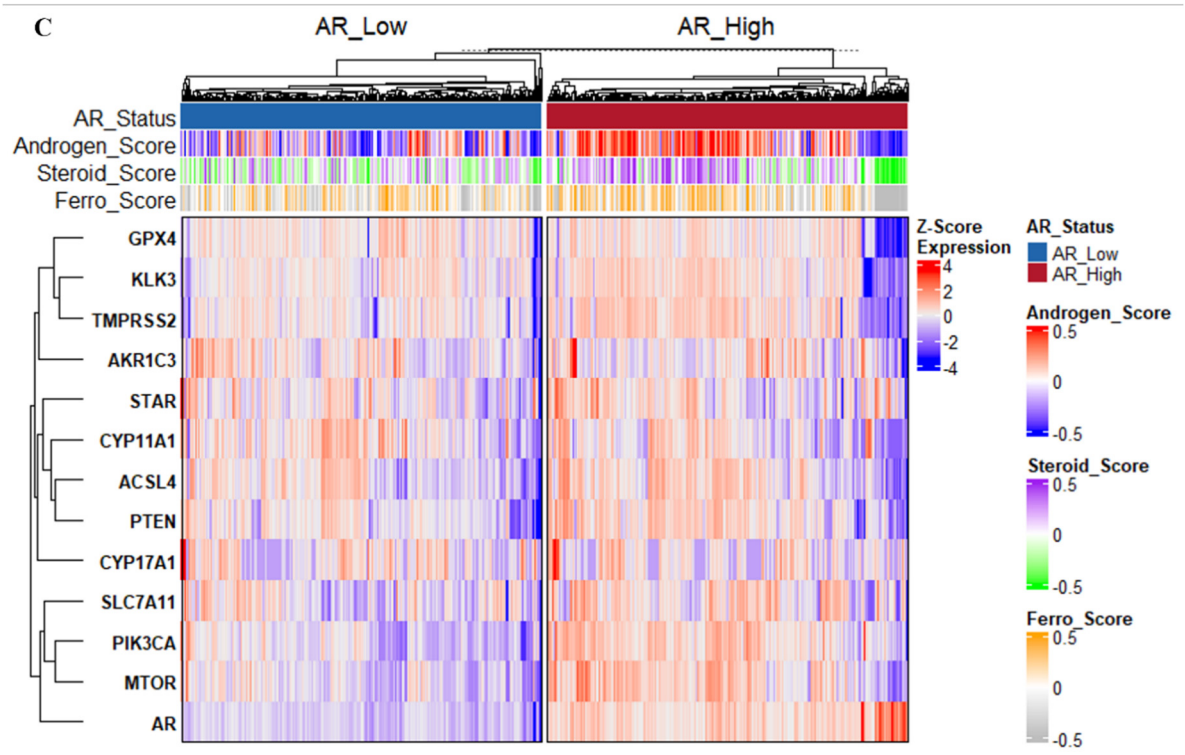

 doi:10.20944/preprints202604.0750.v1

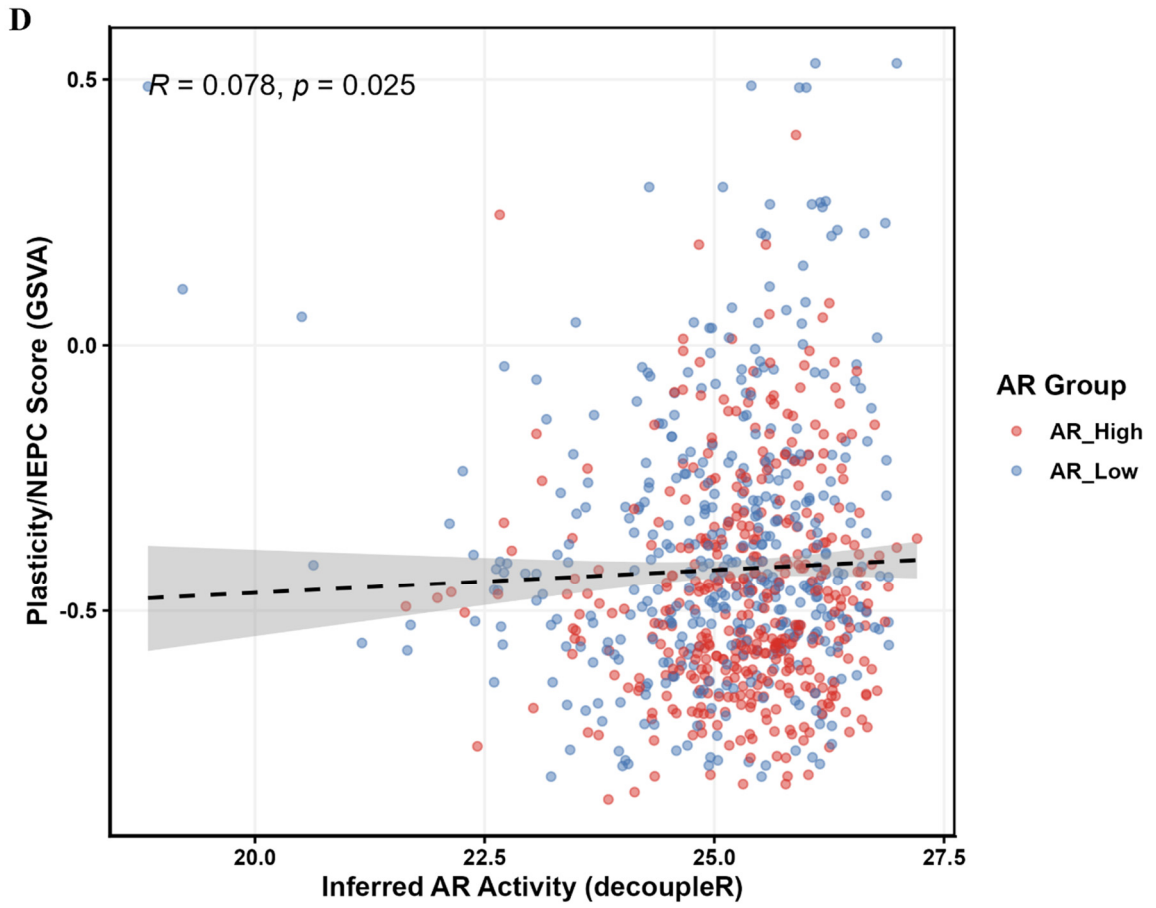

Figure 10. (A) Supervised clustering and heatmap of GSVA Hallmark pathway scores illustrate the global transcriptomic divergence between AR-high (red) and AR-low (blue) cohorts, with the latter showing marked enrichment in developmental (Notch, Wnt β-catenin) and EMT signaling. (B) UMAP visualization maps the functional connectivity between androgen response, ferroptosis, and PI3K signaling, identifying potential regulatory nodes that bridge these metabolic programs. (C) Targeted heatmap profiling of lineage-specific and ferroptosis-associated genes, including KLK3, GPX4, and SLC7A11, reveals distinct expression patterns corresponding to AR status and composite pathway scores. (D) Pearson correlation analysis between inferred AR activity and the Plasticity/NEPC GSVA score (R = 0.078, $p = 0.025$) indicates a significant relationship between AR signaling and cellular plasticity, with the regression line and 95% confidence intervals (gray) highlighting the inherent heterogeneity within the AR-low population.

6.3. Correlation of Steroidogenic Drivers with AR Activity and Clinical Outcome Analysis

To evaluate the clinical relevance of these transcriptomic states, we first examined the contribution of individual steroidogenic enzymes to the inferred androgen signaling activity. Correlation analysis identified SRD5A1 as the primary driver of androgenic signaling ($r = 0.45$), while CYP17A1 exhibited a slight inverse relationship, suggesting a complex rewiring of steroid metabolism (Figure 11A). Despite the clear molecular differences between phenotypes, Kaplan-Meier analysis revealed no significant difference in overall survival probability between the AR-high and AR-low cohorts ($p = 0.79$; *Figure 11B*), likely reflecting the long-term indolence of the disease or the efficacy of subsequent lines of therapy in both groups. To further delineate risk factors, we performed a multivariate Cox proportional hazards analysis (Figure 11C). While the Plasticity Score trended toward increased risk (*HR = 2.00, p = 0.095*), pathological T-stage emerged as the only significant independent predictor of clinical events, with T3/T4 tumors exhibiting a 14.9-fold increase in hazard compared to T2 tumors ($p < 0.0001$).

 doi:10.20944/preprints202604.0750.v1

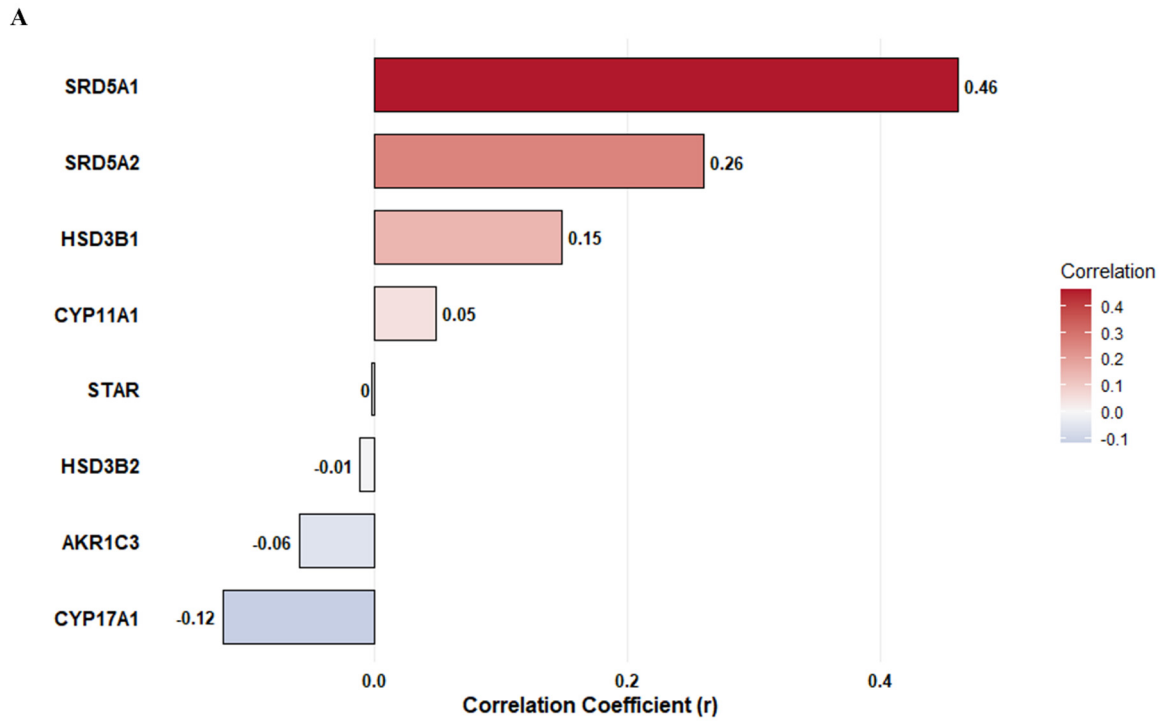

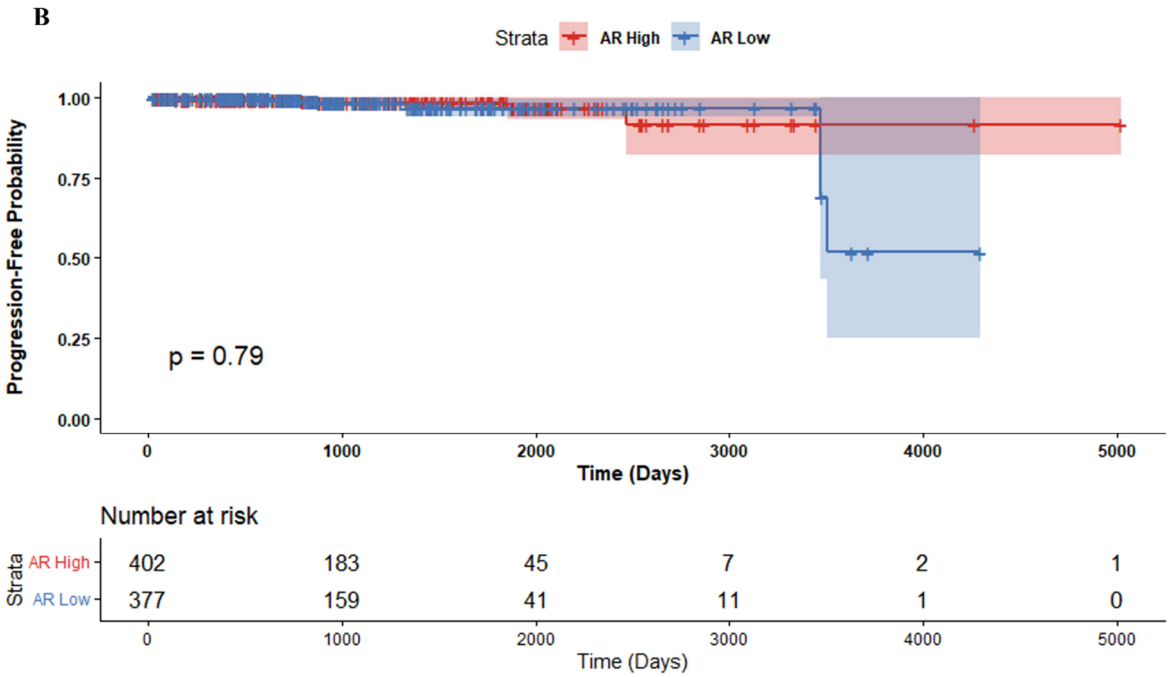

 doi:10.20944/preprints202604.0750.v1

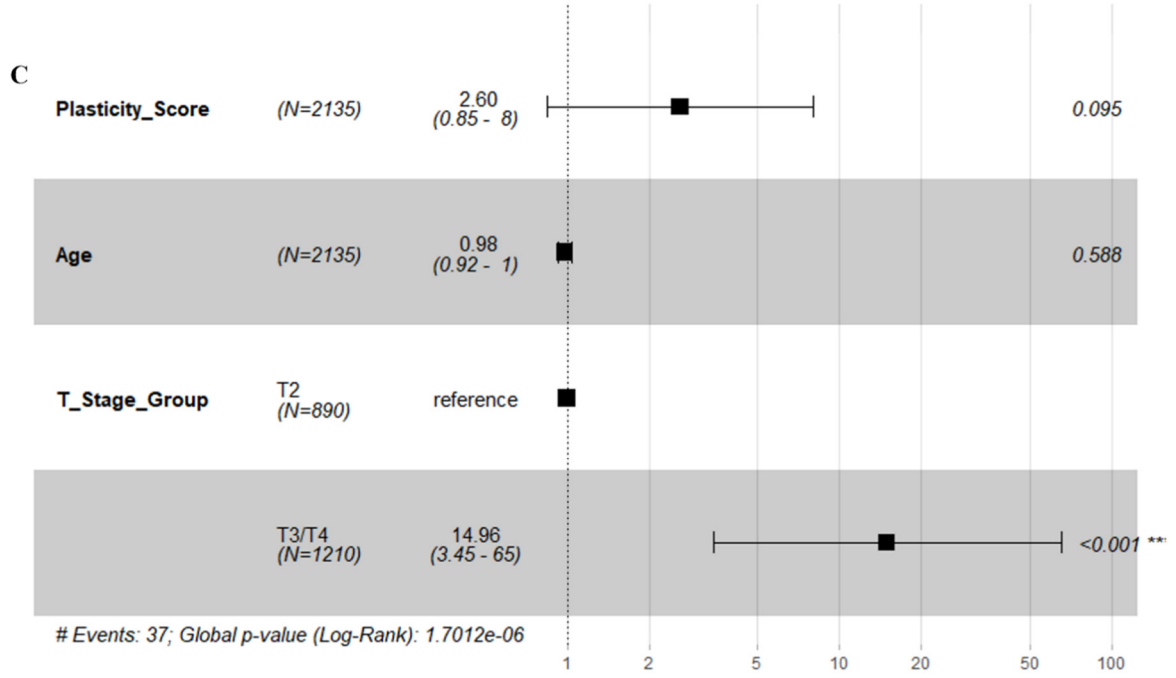

Figure 11. (A) Bar chart illustrates the Pearson correlation coefficients (r) between individual steroidogenic genes and the composite androgen activity score; SRD5A1 emerges as the strongest positive correlation. (B) Kaplan-Meier survival curves comparing AR-high (red) and AR-low (blue) patient cohorts. The log-rank test ($p = 0.79$) indicates no significant difference in survival between the two groups; the "number at risk" for each interval is shown below the plot. (C) A forest plot represents a multivariate Cox proportional hazards model for clinical events. Hazard ratios (HRs), 95% confidence intervals, and p-values are shown for Plasticity Score, Age, and T-Stage Group (T3/T4 vs. reference T2), indicating that advanced tumor stage is the primary driver of clinical risk ($p < 0.0001$).

6. Discussion

Despite major advances in AR-directed therapies, prostate cancer maintains the capacity to adapt to androgen-depleted environments, underscoring the persistence of AR signaling as a central driver of disease progression [8,9,26,36]. CYP17A1 inhibition can effectively suppress systemic androgen synthesis; however, the continued clinical efficacy of AR pathway inhibitors highlights the plasticity of androgen signaling and the ability of tumor cells to utilize residual or locally synthesized steroids [37,38].

In this study, we employed an integrated experimental and computational framework to characterize androgen sensitivity, steroidogenic capacity, and transcriptomic. Functional assays showed that prostate cancer cells retain variable dependence on exogenous DHT, with responses ranging from strongly ligand-sensitive to partially responsive. Rather than exhibiting complete androgen independence, our findings support the notion that LNCaP, VCaP, and 22Rv1 cells sustain AR pathway activity through mixed ligand-dependent and independent mechanisms [39–45].

Transitioning from these in vitro observations to clinical phenotypes, our characterization of 818 PRAD samples revealed that the AR-High cohort is defined not only by classical androgen response but by a coordinated bioenergetic program. GSEA and GSVA identified significant enrichment for Oxidative Phosphorylation, Fatty Acid Metabolism, and MTORC1 signaling in AR-High tumors, suggesting a metabolically hyperactive state. This was further evidenced by the significant upregulation of core signaling nodes such as PIK3CA and mTOR. Conversely, the AR-High phenotype appears more differentiated, showing a marked suppression of EMT and angiogenesis compared to more primitive, undifferentiated state observed in AR-low tumors.

 doi:10.20944/preprints202604.0750.v1

A central strength of this work lies in the direct measurement of steroid production using LC–MS, which provides functional evidence of intratumoral steroidogenic capability. Normal prostate epithelial RWPE-1 cells exhibited minimal steroid production, whereas LNCaP, VCaP, and 22rv1 displayed elevated synthesis of androgen precursors and/or bioactive androgens. The inclusion of H295R adrenal cells served as a positive control for broad steroid biosynthesis and confirmed the assay's sensitivity and dynamic range [20–24,27,28,46,47]. Our results support the concept that prostate cancer cells can acquire partial steroidogenic competency sufficient to sustain AR signaling under androgen-restricted conditions. In the clinical correlation analysis, we identified SRD5A1 as the primary driver of inferred androgenic signaling ($r = 0.45$), confirming our transcriptomic profiling of the cell lines, which showed a coordinated upregulation of enzymes like AKR1C3, HSD3B1/2, and SRD5A1. These enzymes act downstream or independently of CYP17A1, providing a mechanistic basis for continued DHT production. Importantly, these transcriptional changes correspond with measured steroid levels, indicating that metabolic reprogramming translates into functionally relevant output rather than purely transcriptional noise. Also, we identified a novel intersection between androgen signaling and cellular vulnerability. The AR-High group exhibited a distinct shift in ferroptosis-related genes, characterized by upregulation of SLC7A11 and ACSL4, accompanied by significant downregulation of GPX4. This suggests that while AR-high tumors are metabolically robust, they may harbor a specific vulnerability to lipid peroxidation. UMAP multidimensional mapping confirmed this functional intersection, identifying a cluster of ferroptosis and PI3K signaling genes that bridge the AR-High and AR-Low phenotypes.

Heterogeneity across prostate cancer cell models parallels the clinical diversity of castration-resistant prostate cancer, where multiple resistance phenotypes coexist within and between tumors [48–53]. While reduced AR signaling is a hallmark of lineage plasticity, the assessment of the relationship between AR activity and Plastticity/NEPC scores suggest that while a correlation exists, additional epigenetic or stochastic factors likely drive the complete neuroendocrine trans differentiation process. Certain cell lines favor ligand-independent activation via splice variants like AR-V7 (22Rv1), while others (LNCaP, VCaP, and C4-2/C4-2B) capitalize on intratumoral biosynthesis [54–68]. Additionally, models such as VCaP, which harbor AR amplification and increased sensitivity to low androgen concentrations, represent a third phenotype characterized by AR hypersensitivity, while PC3 and DU145 exemplify AR-null states where tumor cells abandon AR dependency altogether and engage in alternative lineage programs. These mechanistic distinctions show that no single cell model adequately captures the spectrum of androgen signaling plasticity. Rather, disease progression appears to be supported by parallel and sometimes co-existing resistance states, reinforcing the importance of employing diverse model systems and cautioning against overgeneralization from studies reliant on isolated models. Despite these deep molecular divergences, Kaplan-Meier analysis revealed no significant difference in overall survival between AR-High and AR-Low cohorts. This depicts long-term indolence of the disease or the efficacy of subsequent therapies, whereas multivariate Cox analysis identified independent predictors of clinical hazard.

This study does possess several limitations. Transcriptomic data capture mRNA-level changes but does not fully account for post-translational regulation or enzyme activity, both of which influence metabolic flux. Additionally, cell line models provide a controlled platform to dissect steroidogenic mechanisms but lack contributions from the tumor microenvironment, stromal signaling, immune components, and systemic steroid pools. Finally, although our findings implicate enhanced steroid metabolism and bioenergetic shifts in maintaining AR signaling, causal inference will require targeted perturbation of steroidogenic and ferroptotic pathways in future work.

7. Conclusion

The present study fundamentally reframes the paradigm of intracrine metabolism in castration-resistant prostate cancer. By integrating high-resolution liquid chromatography-mass spectrometry with deep transcriptomics and large-scale clinical profiling, we demonstrate that prostate cancer

 doi:10.20944/preprints202604.0750.v1

adapts to androgen-restricted environments not by developing autonomous *de novo* steroidogenic factories, but by rewiring its metabolism into a highly efficient converter system.

Our data definitively challenges the persistent tumor-as-gonad hypothesis. We show that canonical *in vitro* models universally lack the necessary *CYP17A1* enzymatic machinery and fail to synthesize androgens from cholesterol. Rather, they act as high-capacity precursor scavengers, utilizing hyperactivated downstream enzymes such as *HSD3B1* and *AKR1C3* to sustain androgen receptor (AR) signaling. Concurrently, we uncover a ubiquitous Cortisol Void, the distinct silencing of *CYP21A2* activity in malignant phenotypes. This highly significant metabolic lesion likely serves a dual oncogenic purpose: preventing the synthesis of differentiation-inducing glucocorticoids while shunting available precursors toward the synthesis of mitogenic androgens.

Crucially, the translation of these *in vitro* metabolic blueprints into a clinical cohort of 844 PRAD patients validated these dependencies on a global scale. We identified that the clinical landscape is bifurcated into distinct evolutionary trajectories: an AR-High phenotype fueled by intense metabolic hyperactivity (oxidative phosphorylation and fatty acid metabolism) and an AR-Low state marked by extensive lineage plasticity. The neuroendocrine plasticity score emerged as a potent, independent predictor of disease progression (HR = 2.41), emphasizing that the escape from canonical AR dependency represents a lethal clinical transition.

These findings mandate a fundamental shift in therapeutic strategy. Because tumors can circumvent castrate environments by capitalizing on circulating precursor pools, solely targeting upstream *CYP17A1* biosynthesis is insufficient. Overcoming advanced resistance necessitates combination approaches targeting downstream conversion nodes (such as *AKR1C3* and *HSD3B1* inhibitors) to comprehensively block DHT formation. Furthermore, uncovering the specific vulnerabilities of these phenotypic states, such as the dysregulation of ferroptosis-related genes in AR-High tumors and compensatory PI3K/AKT activation, provides a rational basis for biomarker-guided combinatorial therapies. Ultimately, recognizing the prostate tumor as a broken but adaptive metabolic pathway provides a robust roadmap for the development of next-generation interventions capable of anticipating and neutralizing the evolutionary plasticity of CRPC.

Supplementary Materials: The following supporting information can be downloaded at the website of this paper posted on Preprints.org.

Author contributions: **A.V.P.** conceived and designed the study, provided overall supervision, acquired funding, and edited the final draft of the manuscript. **T.D.T.** designed and performed the high-resolution mass spectrometric analysis of steroids, conducted metabolomic data analysis, and contributed to the writing and critical editing of the manuscript. **J.Y.** performed the *in vitro* experiments (including cell viability and kinetic assays), conducted the transcriptomic and bioinformatic data analysis, prepared all images and tables, and wrote the initial draft of the manuscript. All authors discussed the results, reviewed the manuscript, and approved the final submitted version.

Data availability Statement: All data described are available in figures or database links in the text.

Acknowledgements: We thank Prof. Mark Rubin (Department of Biomedical Research, University of Bern, Switzerland) for providing PC3, VCaP, DU145, and RWPE-1 cell lines. This research was supported by the CANCER RESEARCH SWITZERLAND grant number KFS-5557-02-2022 to AVP.

Disclosure statement: *The authors report there are no competing interests to declare.*

References

1. Pinto, F., et al., *Mechanisms of Resistance to Second-Generation Antiandrogen Therapy for Prostate Cancer: Actual Knowledge and Perspectives.* Med Sci (Basel), 2022. **10**(2).
2. Karantanos, T., et al., *Prostate cancer progression after androgen deprivation therapy: mechanisms of castrate resistance and novel therapeutic approaches.* Oncogene 2013 32:49, 2013–06–10. **32**(49).

 doi:10.20944/preprints202604.0750.v1

3. Choi, E., et al., *Evolution of Androgen Deprivation Therapy (ADT) and Its New Emerging Modalities in Prostate Cancer: An Update for Practicing Urologists, Clinicians and Medical Providers.* Res Rep Urol, 2022. **14**: p. 87–108.
4. Ryan, C.J., et al., *Abiraterone in Metastatic Prostate Cancer without Previous Chemotherapy.* New England Journal of Medicine, 2013–01–10. **368**(2).
5. James, N.D., et al., *Abiraterone for Prostate Cancer Not Previously Treated with Hormone Therapy.* N Engl J Med, 2017. **377**(4): p. 338–351.
6. de Bono, J.S., et al., *Abiraterone and Increased Survival in Metastatic Prostate Cancer.* New England Journal of Medicine, 2011–05–26. **364**(21).
7. Sprenger, C.C. and S.R. Plymate, *The link between androgen receptor splice variants and castration-resistant prostate cancer.* Horm Cancer, 2014. **5**(4): p. 207–17.
8. Watson, P.A., V.K. Arora, and C.L. Sawyers, *Emerging mechanisms of resistance to androgen receptor inhibitors in prostate cancer.* Nat Rev Cancer, 2015. **15**(12): p. 701–11.
9. Penning, T.M., *Mechanisms of drug resistance that target the androgen axis in castration resistant prostate cancer (CRPC).* The Journal of Steroid Biochemistry and Molecular Biology, 2015. **153**: p. 105–113.
10. Sobel, R.E. and M.D. Sadar, *Cell lines used in prostate cancer research: a compendium of old and new lines--part 2.* J Urol, 2005. **173**(2): p. 360–72.
11. Sobel, R.E. and M.D. Sadar, *Cell lines used in prostate cancer research: a compendium of old and new lines--part 1.* J Urol, 2005. **173**(2): p. 342–59.
12. Smith, R., et al., *Enzalutamide response in a panel of prostate cancer cell lines reveals a role for glucocorticoid receptor in enzalutamide resistant disease.* Sci Rep, 2020. **10**(1): p. 21750.
13. Saranyutanon, S., et al., *Cellular and Molecular Progression of Prostate Cancer: Models for Basic and Preclinical Research.* Cancers (Basel), 2020. **12**(9).
14. Russell, P.J. and E.A. Kingsley, *Human prostate cancer cell lines.* Methods Mol Med, 2003. **81**: p. 21–39.
15. Moya, L., et al., *Characterisation of cell lines derived from prostate cancer patients with localised disease.* Prostate Cancer and Prostatic Diseases 2023 26:3, 2023–06–01. **26**(3).
16. Dagvadorj, A., et al., *Androgen-regulated and highly tumorigenic human prostate cancer cell line established from a transplantable primary CWR22 tumor.* Clin Cancer Res, 2008. **14**(19): p. 6062–72.
17. Abate-Shen, C. and F. Nunes de Almeida, *Establishment of the LNCaP Cell Line - The Dawn of an Era for Prostate Cancer Research.* Cancer Res, 2022. **82**(9): p. 1689–1691.
18. Bello, D., et al., *Androgen responsive adult human prostatic epithelial cell lines immortalized by human papillomavirus 18.* Carcinogenesis, 1997. **18**(6): p. 1215–23.
19. Wang, T. and W.E. Rainey, *Human adrenocortical carcinoma cell lines.* Mol Cell Endocrinol, 2012. **351**(1): p. 58–65.
20. Udhane, S., et al., *Differential regulation of human 3beta-hydroxysteroid dehydrogenase type 2 for steroid hormone biosynthesis by starvation and cyclic AMP stimulation: studies in the human adrenal NCI-H295R cell model.* PLoS One, 2013. **8**(7): p. e68691.
21. Lichtenauer, U.D., et al., *Characterization of NCI-H295R cells as an in vitro model of hyperaldosteronism.* Horm Metab Res, 2013. **45**(2): p. 124–9.
22. Hirsch, A., et al., *Role of AMP-activated protein kinase on steroid hormone biosynthesis in adrenal NCI-H295R cells.* PLoS One, 2012. **7**(1): p. e30956.
23. Nishi, H., H. Arai, and T. Momiyama, *NCI-H295R, a human adrenal cortex-derived cell line, expresses purinergic receptors linked to Ca(2)(+)-mobilization/influx and cortisol secretion.* PLoS One, 2013. **8**(8): p. e71022.
24. Samandari, E., et al., *Human adrenal corticocarcinoma NCI-H295R cells produce more androgens than NCI-H295A cells and differ in 3beta-hydroxysteroid dehydrogenase type 2 and 17,20 lyase activities.* J Endocrinol, 2007. **195**(3): p. 459–72.
25. Yakubu, J., et al., *Nanoparticles with curcumin and piperine modulate steroid biosynthesis in prostate cancer.* Sci Rep, 2025. **15**(1): p. 13613.
26. Sharma, K., et al., *Effect of Essential Oil Components on the Activity of Steroidogenic Cytochrome P450.* Biomolecules, 2024. **14**(2).
27. Wrobel, T.M., et al., *Pyridine indole hybrids as novel potent CYP17A1 inhibitors.* J Enzyme Inhib Med Chem, 2025. **40**(1): p. 2463014.

 doi:10.20944/preprints202604.0750.v1

28. Sharma, K., et al., *Effect of Essential Oil Components on the Activity of Steroidogenic Cytochrome P450.* Biomolecules 2024, Vol. 14, Page 203, 2024–02–08. **14**(2).
29. Jensen, M.A., et al., *The NCI Genomic Data Commons as an engine for precision medicine.* Blood, 2017. **130**(4): p. 453–459.
30. Heath, A.P., et al., *The NCI Genomic Data Commons.* Nat Genet, 2021. **53**(3): p. 257–262.
31. Ritchie, M.E., et al., *limma powers differential expression analyses for RNA-sequencing and microarray studies.* Nucleic Acids Res, 2015. **43**(7): p. e47.
32. Hanzelmann, S., R. Castelo, and J. Guinney, *GSVA: gene set variation analysis for microarray and RNA-seq data.* BMC Bioinformatics, 2013. **14**(1): p. 7.
33. Subramanian, A., et al., *Gene set enrichment analysis: a knowledge-based approach for interpreting genome-wide expression profiles.* Proc Natl Acad Sci U S A, 2005. **102**(43): p. 15545–50.
34. Labanca, E., et al., *Prostate cancer castrate resistant progression usage of non-canonical androgen receptor signaling and ketone body fuel.* Oncogene, 2021. **40**(44): p. 6284–6298.
35. Chen, H., F. Lyu, and X. Gao, *Advances in ferroptosis for castration-resistant prostate cancer treatment: novel drug targets and combination therapy strategies.* Prostate Cancer Prostatic Dis, 2026. **29**(1): p. 36–46.
36. Watson, P.A., et al., *Constitutively active androgen receptor splice variants expressed in castration-resistant prostate cancer require full-length androgen receptor.* Proc Natl Acad Sci U S A, 2010. **107**(39): p. 16759–65.
37. Fizazi, K., et al., *Abiraterone plus Prednisone in Metastatic, Castration-Sensitive Prostate Cancer.* N Engl J Med, 2017. **377**(4): p. 352–360.
38. Singhal, G., et al., *Advancing Prostate Cancer Treatment: Innovations and Challenges in Imm.* Cancer Treatment and Research, 2025.
39. Zhang, X., et al., *Androgen Receptor Variants Occur Frequently in Castration Resistant Prostate Cancer Metastases.* PLOS ONE, 17 Nov 2011. **6**(11).
40. TM, P., *Mechanisms of drug resistance that target the androgen axis in castration resistant prostate cancer (CRPC).* The Journal of Steroid Biochemistry and Molecular Biology, 2015/05/29. **153**.
41. Hussain, M., et al., *Metastatic Hormone-Sensitive Prostate Cancer and Combination Treatment Outcomes.* JAMA Oncology, 2024/06/01. **10**(6).
42. Chandrasekar, T., et al., *Mechanisms of resistance in castration-resistant prostate cancer (CRPC).* Translational Andrology and Urology, 2015/06. **4**(3).
43. Amaral, T.M., et al., *Castration-resistant prostate cancer: mechanisms, targets, and treatment.* Prostate Cancer, 2012. **2012**(1): p. 327253.
44. Schalken, J. and J.M. Fitzpatrick, *Enzalutamide: targeting the androgen signalling pathway in metastatic castration-resistant prostate cancer.* BJU International, 2016/02/01. **117**(2).
45. Barata, P.C. and A.O. Sartor, *Metastatic castration-sensitive prostate cancer: Abiraterone, docetaxel, or.* Cancer, 2019. **125**(11): p. 1777–1788.
46. Wrobel, T.M., et al., *Exploring the Potential of Sulfur Moieties in Compounds Inhibiting Steroidogenesis.* Biomolecules, 2023. **13**(9).
47. Yakubu, J., et al., *Nanoparticles with curcumin and piperine modulate steroid biosynthesis in prostate cancer.* Scientific Reports 2025 15:1, 2025–04–19. **15**(1).
48. Wu, X., et al., *Current mouse and cell models in prostate cancer research.* Endocr Relat Cancer, 2013. **20**(4): p. R155–70.
49. Sampson, N., et al., *In vitro model systems to study androgen receptor signaling in prostate cancer.* Endocr Relat Cancer, 2013. **20**(2): p. R49–64.
50. Hayward, S.W., et al., *Establishment and characterization of an immortalized but non-transformed human prostate epithelial cell line: BPH-1.* In Vitro Cell Dev Biol Anim, 1995. **31**(1): p. 14–24.
51. Cunningham, D. and Z. You, *In vitro and in vivo model systems used in prostate cancer research.* J Biol Methods, 2015. **2**(1).
52. Ahmed, K., et al., *Comparison of baseline global gene expression profiles of prostate cancer cell lines LNCaP and DU145.* BMC Res Notes, 2024. **17**(1): p. 398.
53. Moya, L., et al., *Characterisation of cell lines derived from prostate cancer patients with localised disease.* Prostate Cancer Prostatic Dis, 2023. **26**(3): p. 614–624.

 doi:10.20944/preprints202604.0750.v1

54. Pujana-Vaquerizo, M., et al., *Metabolic adaptations in prostate cancer.* British Journal of Cancer 2024 131:8, 2024–07–05. **131**(8).
55. Eksi, S.E., et al., *Epigenetic loss of heterogeneity from low to high grade localized prostate tumours.* Nat Commun, 2021. **12**(1): p. 7292.
56. Ferretti, S., et al., *Metastatic Castration-Resistant Prostate Cancer: Insights on Current Therapy and Promising Experimental Drugs.* Res Rep Urol, 2023. **15**: p. 243–259.
57. Ma, B., et al., *De Novo Design of an Androgen Receptor DNA Binding Domain-Targeted peptide PROTAC for Prostate Cancer Therapy.* Advanced Science, 2022. **9**(28): p. 2201859.
58. Verma, K., et al., *AKR1C3 Inhibitor KV-37 Exhibits Antineoplastic Effects and Potentiates Enzalutamide in Combination Therapy in Prostate Adenocarcinoma Cells.* Molecular Cancer Therapeutics, 2018. **17**(9): p. 1833–1845.
59. Ning, S., et al., *LX1 Dual Targets AR Variants and AKR1C3 in Advanced Prostate Cancer Therapy.* Cancer Research, 2024. **84**(21): p. 3617–3628.
60. Maddeboina, K., et al., *Aldo-Keto Reductase 1C3 Inhibitor Prodrug Improves Pharmacokinetic Profile and Demonstrates In Vivo Efficacy in a Prostate Cancer Xenograft Model.* Journal of Medicinal Chemistry, 2023. **66**(14): p. 9894–9915.
61. Carmona, A.V., et al., *Discovery of an Aldo-Keto reductase 1C3 (AKR1C3) degrader.* Communications Chemistry, 2024. **7**(1): p. 95.
62. Lubik, A.A., et al., *IGF2 increases de novo steroidogenesis in prostate cancer cells.* Endocrine-Related Cancer, 2013–04–01. **20**(2).
63. Simpson, K., et al., *Metformin in overcoming enzalutamide resistance in castration-resistant prostate cancer.* J Pharmacol Exp Ther, 2025. **392**(1): p. 100034.
64. Pang, J.-p., et al., *Discovery of novel antagonists targeting the DNA binding domain of androgen receptor by integrated docking-based virtual screening and bioassays.* Acta Pharmacologica Sinica, 2022. **43**(1): p. 229–239.
65. Song, K., et al., *Androgenic control of transforming growth factor-beta signaling in prostate epithelial cells through transcriptional suppression of transforming growth factor-beta receptor II.* Cancer Res, 2008. **68**(19): p. 8173–82.
66. Pfitzenmaier, J., et al., *Characterization of C4-2 prostate cancer bone metastases and their response to castration.* J Bone Miner Res, 2003. **18**(10): p. 1882–8.
67. Denmeade, S.R., et al., *Dissociation between androgen responsiveness for malignant growth vs. expression of prostate specific differentiation markers PSA, hK2, and PSMA in human prostate cancer models.* Prostate, 2003. **54**(4): p. 249–57.
68. Bisson, I. and D.M. Prowse, *WNT signaling regulates self-renewal and differentiation of prostate cancer cells with stem cell characteristics.* Cell Res, 2009. **19**(6): p. 683–97.